

RESEARCH ARTICLE

Wnt proteins contribute to neuromuscular junction formation through distinct signaling pathways

Julien Messéant^{1,*}, Jérôme Ezan^{2,3}, Perrine Delers¹, Konstantin Glebov^{2,3,‡}, Carmen Marchiol⁴, Franck Lager⁴, Gilles Renault⁴, Fadel Tissir⁵, Mireille Montcouquiol^{2,3}, Nathalie Sans^{2,3}, Claire Legay¹ and Laure Strohlic^{1,*}§

ABSTRACT

Understanding the developmental steps that shape formation of the neuromuscular junction (NMJ) connecting motoneurons to skeletal muscle fibers is crucial. Wnt morphogens are key players in the formation of this specialized peripheral synapse, but their individual and collaborative functions and downstream pathways remain poorly understood at the NMJ. Here, we demonstrate through Wnt4 and Wnt11 gain-of-function studies in cell culture or in mice that Wnts enhance acetylcholine receptor (AChR) clustering and motor axon outgrowth. By contrast, loss of Wnt11 or Wnt-dependent signaling *in vivo* decreases AChR clustering and motor nerve terminal branching. Both Wnt4 and Wnt11 stimulate AChR mRNA levels and AChR clustering downstream of activation of the β -catenin pathway. Strikingly, Wnt4 and Wnt11 co-immunoprecipitate with Vangl2, a core component of the planar cell polarity (PCP) pathway, which accumulates at embryonic NMJs. Moreover, mice bearing a *Vangl2* loss-of-function mutation (loop-tail) exhibit fewer AChR clusters and overgrowth of motor axons bypassing AChR clusters. Together, our results provide genetic and biochemical evidence that Wnt4 and Wnt11 cooperatively contribute to mammalian NMJ formation through activation of both the canonical and Vangl2-dependent core PCP pathways.

KEY WORDS: Neuromuscular junction, β -catenin signaling, Planar cell polarity, Wnt, Vangl2, Mouse

INTRODUCTION

Formation of the vertebrate neuromuscular junction (NMJ), a peripheral cholinergic synapse between motoneurons and skeletal muscle fibers, relies on the accurate recognition and apposition of presynaptic motoneurons on postsynaptic muscle targets, a process achieved by a variety of organizing signals from both partners (Tintignac et al., 2015). Growing evidence in several vertebrate species, using both *in vitro* and *in vivo* models, suggests that Wnt morphogens act as regulators of NMJ initiation and/or formation (Gordon et al., 2012; Henriquez et al., 2008; Jing et al., 2009; Messéant et al., 2015; Packard et al., 2002; Strohlic et al., 2012;

Zhang et al., 2012). Yet, Wnt function and the molecular mechanisms through which Wnts collaborate at the mammalian NMJ remain elusive and controversial.

Wnts are known to activate a canonical signaling pathway that is β -catenin (Ctnnb1) dependent, as well as several non-canonical pathways such as the core planar cell polarity (PCP) pathway (Nusse, 2012). At the vertebrate NMJ, Wnt ligands transduce their signals through activation of the receptor complex formed by the muscle-specific tyrosine kinase MuSK and low-density lipoprotein receptor-related protein 4 (Lrp4) and through the activation of classical Frizzled (Fzd) receptors (Avilés et al., 2014; Zhang et al., 2012; Strohlic et al., 2012; Gordon et al., 2012; Messéant et al., 2015). The MuSK-Lrp4 complex constitutes the central scaffold for the formation of the neuromuscular synapse (DeChiara et al., 1996; Kim et al., 2008; Weatherbee et al., 2006; Zhang et al., 2008). Activation of this complex is required for: (1) the early, nerve-independent muscle pre-patterning, as characterized by acetylcholine receptor (AChR) aggregation in the prospective synaptic region of the muscle surface that helps to guide growing motor axons towards their final target; and (2) the late, nerve-dependent differentiation and maturation of the synapse (Tintignac et al., 2015). This later step is orchestrated by the release of a nerve secreted isoform of agrin, which binds to muscle Lrp4 leading to activation of MuSK and AChR clustering in the postsynaptic membrane (Kim et al., 2008; Zhang et al., 2008, 2011; Zong et al., 2012).

Among the 19 Wnts currently identified in mammals, Wnt2, 3a, 4, 6, 7b, 9a and 11 directly interact with MuSK but only Wnt4, 9a and 11 enhance AChR clustering in muscle cells (Barik et al., 2014; Strohlic et al., 2012; Zhang et al., 2012). In zebrafish, both Wnt4a and Wnt11r initiate muscle pre-patterning, probably by stimulating PCP-dependent MuSK endocytosis in muscle cells (Gordon et al., 2012; Jing et al., 2009). In mice, although recent data have challenged the role of Wnts at the NMJ (Remédio et al., 2016; discussed below), we have demonstrated that Wnt4 contributes to muscle pre-patterning (Strohlic et al., 2012). Wnt signaling is also required for later steps of vertebrate NMJ differentiation. For example, dishevelled 1 (Dvl1), a hub for Wnt signaling, interacts with MuSK and plays several roles during NMJ formation (Henriquez et al., 2008; Jing et al., 2009; Luo et al., 2002; Wang et al., 2014). Wnt3 expressed by motoneurons enhances AChR clustering in the developing chicken wing and agrin-induced AChR clustering in cultured myotubes through a non-canonical signaling pathway (Henriquez et al., 2008). By contrast, Wnt3a disperses agrin-induced AChR clusters by downregulating rapsyn expression in a β -catenin-dependent manner in muscle cell culture (Wang et al., 2008). In addition, muscle β -catenin gain- or loss-of-function in mice revealed its role in pre- and postsynaptic differentiation consistent with a critical level of β -catenin expression being required for the proper formation of the NMJ (Li et al., 2008; Liu et al., 2012; Wang and Luo, 2008; Wu et al., 2012a, 2015).

¹CNRS UMR 8119, CNRS UMR 8194, Université Paris Descartes, PRES Sorbonne Paris Cité, Paris 75270 Cedex 06, France. ²INSERM, Neurocentre Magendie, U1215, Bordeaux 33077, France. ³Université de Bordeaux, Neurocentre Magendie, U1215, Bordeaux 33077, France. ⁴INSERM U1016, Institut Cochin, Université Paris Descartes, PRES Sorbonne Paris Cité, Paris 75014, France. ⁵Université Catholique de Louvain, Institute of Neuroscience, Brussels B1200, Belgium.

*Present address: Institut du Cerveau et de la Moelle épinière-ICM CNRS UMR 7225-InsERM U1127-UPMC UMR_S1127, Paris 75013, France. ‡Present address: Department of Neurology, University Hospital of Bonn, Bonn 53127, Germany.

§Author for correspondence (laure.strohlic@inserm.fr)

 L.S., 0000-0001-5373-4284

Here, we have used a set of mutant mice, as well as newly designed *in vivo* tools and biochemical assays, to identify the signaling pathways activated by Wnt/receptor interaction and their function in pre- and postsynaptic differentiation of mammalian NMJs. We show that Wnt11 cooperates with Wnt4 to enhance AChR subunit mRNA levels and aneural AChR clustering in cultured muscle cells, in part through activation of β -catenin signaling. In addition, *in vivo* application of both Wnt4 and Wnt11 before NMJs begin to form enhances AChR clustering and motor axon outgrowth. By contrast, lack of Wnt11 or inhibition of all Wnt-dependent signaling *in vivo* decreases AChR clustering and nerve terminal arborization. Specific inhibition of the Wnt canonical pathway similarly affects AChR distribution but not axonal branching, suggesting that distinct branches of Wnt signaling regulate nerve terminal arborization. Interestingly, a significant number of axons fail to terminate at AChR clusters and grow exuberantly beyond the prepatterned region of the muscle. Finally, we show that: (1) both Wnt11 and Wnt4 co-immunoprecipitate with Vangl2, a key component of the core PCP pathway; (2) Vangl2 accumulates at embryonic NMJs; and (3) mice bearing the *Vangl2* loss-of-function mutation loop-tail (*Vangl2^{Lp/Lp}*) exhibit disrupted AChR clusters and axon outgrowth that bypasses AChR clusters. Taken together, our results provide compelling evidence that the coordinate action of Wnt4 and Wnt11 regulates NMJ formation through activation of both the canonical and Vangl2-dependent PCP pathways.

RESULTS

Wnt4 and Wnt11 cooperatively enhance AChR clustering

In view of the complex and still debated role of Wnt4 and Wnt11 in vertebrate NMJ formation (Gordon et al., 2012; Jing et al., 2009; Messéant et al., 2015; Remédio et al., 2016; Strohlic et al., 2012), we investigated events downstream of Wnt4 and Wnt11 and whether they cooperate to induce AChR clustering. Wnt11 alone is

known to enhance AChR clustering *in vitro*; however, conflicting results have been reported regarding the effect of Wnt4 recombinant protein or of Wnt4-conditioned medium treatment of muscle cells on AChR clustering *in vitro* (Strohlic et al., 2012; Zhang et al., 2012). We used a mouse muscle cell line generated in our laboratory that carries a temperature-sensitive large T oncogene. Stages of muscle differentiation have been described previously (see Materials and Methods; Cartaud et al., 2004; Sigoillot et al., 2010, 2016). We quantified *Wnt11* mRNA expression by RT-PCR at three muscle cell stages. These data revealed that, similarly to *Wnt4* (Strohlic et al., 2012), *Wnt11* mRNA levels are strongly upregulated at T2 (when AChR clusters are observed) as compared with T1 (early-formed myotubes without AChR clusters) and then downregulated at T3 (mature contracting myotubes with AChR and acetylcholinesterase clusters). Thus, *Wnt11* is expressed by muscle cells when AChR clusters begin to form (Fig. 1A).

T2 muscle cells were treated for 16 h with concentrations of Wnt4 or Wnt11 ranging from 2.5 ng/ml to 20 ng/ml. Treatment with 2.5 ng/ml Wnt4 and/or Wnt11 did not result in a statistically significant effect on AChR clustering (Fig. 1B). However, each Wnt induced a significant, dose-dependent increase in AChR clustering beginning at 5 ng/ml, with maximal AChR clusters per myotube reached at 10 ng/ml (62% for Wnt4 and 73% for Wnt11; Fig. 1B). Importantly, when Wnt4 and Wnt11 were applied together, a significant increase in the number of AChR clusters (~45% for 5 ng/ml, ~80% for 10 ng/ml and ~50% for 20 ng/ml) was observed as compared with myotubes treated with Wnt4 or Wnt11 separately. In addition, combined suboptimal doses of each Wnt (2.5 ng/ml) did not induce a larger increase in the number of AChR clusters compared with Wnt4 or Wnt11 applied separately (5 ng/ml) (Fig. 1B). These results indicate that the two Wnts act cooperatively to induce AChR clustering and suggest that Wnt effects on AChR clustering vary according to the Wnt concentration used. This might explain some of the reported differences in Wnt

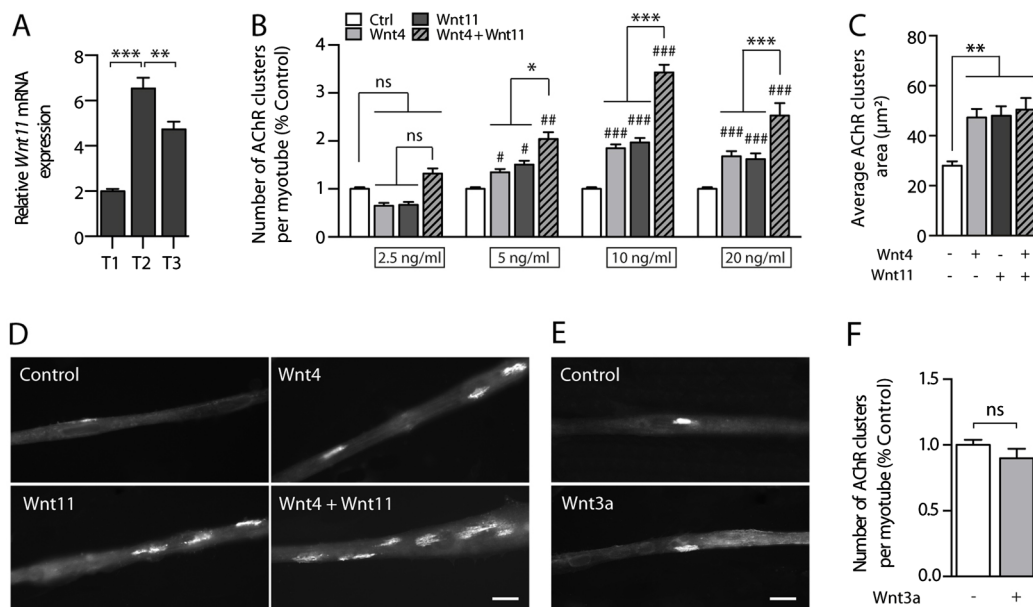


Fig. 1. Wnt4 and Wnt11 cooperatively enhance AChR clustering *in vitro*. (A) Real-time RT-PCR quantification of relative *Wnt11* mRNA expression during myotube differentiation at three muscle stages: T1, myotube formation; T2, visualization of AChR clusters; and T3, late muscle differentiation. (B) Quantification of AChR cluster number in control myotubes or in those treated with increasing concentrations of Wnt4 and/or Wnt11 for 16 h. (C) Average AChR cluster area. (D,E) Examples of myotubes stained with α -bungarotoxin (BTX) from control or embryos treated with Wnt4 and/or Wnt11 or Wnt3a (10 ng/ml) for 16 h. (F) Number of AChR clusters per myotube. At least 80 myotubes were analyzed for each condition. ns, non-significant; *,# P <0.05; **,### P <0.01; ***,#### P <0.001 (#: compared with untreated myotubes); Mann–Whitney *U*-test or one-way ANOVA. Scale bars: 20 μm .

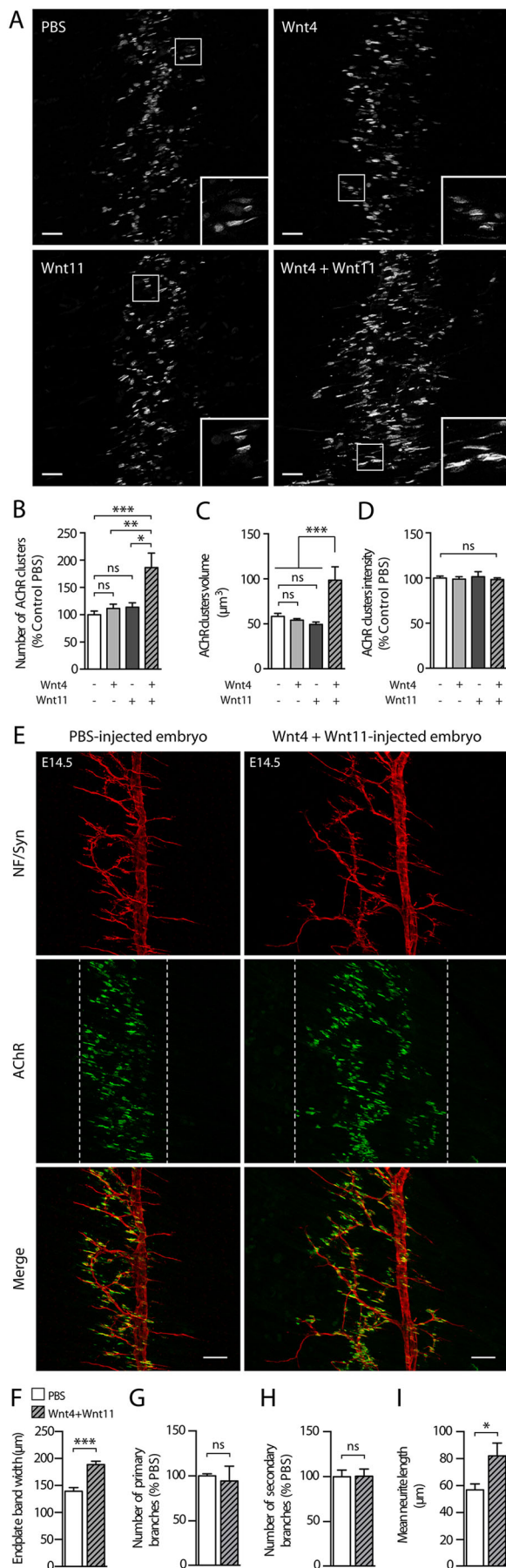


Fig. 2. Wnt4 and Wnt11 cooperate to enhance AChR clustering and presynaptic axon outgrowth *in vivo*. (A) Confocal images of whole-mount left hemidiaphragms from E14.5 PBS-injected or Wnt4 and/or Wnt11-injected embryos stained with BTX. Insets are high-magnification views of AChR clusters. (B-D) Quantitative analysis of AChR cluster number (B), volume (C) and fluorescence intensity (D). (E) Confocal images of whole-mount left hemidiaphragms from E14.5 PBS-injected or Wnt4/Wnt11-injected embryos stained with neurofilament (NF, red) and synaptophysin (Syn, red) antibodies together with BTX (green). White dashed lines delineate the synaptic endplate band. (F-I) Quantification of endplate band width (F), number of primary (G) and secondary (H) nerve branches and mean axon length (I). $n=5$ embryos per condition. ns, non-significant; * $P<0.05$, ** $P<0.01$, *** $P<0.001$; Mann-Whitney U -test or one-way ANOVA. Scale bars: 40 μm .

effects on AChR clusters where the concentrations were not carefully controlled.

We further quantified morphological aspects of AChR clusters following Wnt4 and/or Wnt11 treatment overnight at maximal concentration (10 ng/ml; Fig. 1C,D). Wnt4 and/or Wnt11 treatment enhanced the size of AChR clusters similarly, as compared with control myotubes (Fig. 1C). To assess the specificity of Wnt4- and Wnt11-induced AChR clustering, myotubes were treated overnight with Wnt3a (10 ng/ml), which is known to have no effect on basal AChR clustering in cultured myotubes (Henriquez et al., 2008). As expected, Wnt3a did not affect the number of AChR clusters compared with control myotubes (Fig. 1E,F).

We then examined whether both Wnts stimulate AChR clustering *in vivo*. To directly target the embryonic diaphragm, we used ultrasound-guided injections of Wnt4 and/or Wnt11 in live mouse embryos (see Materials and Methods; Fig. S1), which allowed us to specifically assess protein function *in vivo* in a restricted spatiotemporal window (Nieman and Turnbull, 2010; Slevin et al., 2006). A single injection of each Wnt (50 $\mu\text{g/ml}$) or of both together (25 $\mu\text{g/ml}$) was performed directly into the peritoneum of E12.5 embryos to target the diaphragm before NMJs started to form, with analysis 2 days later (E14.5) to visualize their *in vivo* effects during early stages of NMJ formation. Whole-mount diaphragms were labeled with α -bungarotoxin (BTX) to detect AChR clusters, together with a mixture of antibodies against synaptophysin (Syn) and neurofilament (NF) to visualize nerve terminals and axonal branches, respectively (Fig. 2A,E). Compared with PBS-injected controls, injection of Wnt4 or Wnt11 alone did not enhance AChR clustering. However, embryos injected with both Wnt4 and Wnt11 displayed increases in the number (+131%) and volume (+44%), but not fluorescence intensity, of AChR clusters (Fig. 2B-D). Moreover, in PBS-injected embryos synapses were concentrated in a narrow band and AChR clusters appeared as a thin line in the middle of each hemidiaphragm, whereas in embryos injected with both Wnt4 and Wnt11 most of the AChR clusters were distributed in a 1.3-fold wider area (Fig. 2E,F). Injection of Wnt4 or Wnt11 alone did not affect nerve terminal arborization and axonal outgrowth (data not shown), whereas injection of both Wnt4 and Wnt11 increased the mean axon length by 44% without affecting the number of primary and secondary branches (Fig. 2E,G-I). Collectively, these data support a cooperative function of Wnt4 and Wnt11 in AChR clustering and axonal outgrowth.

Loss of Wnt function impairs NMJ formation

The above results prompted us to study the effect of loss of Wnt function during NMJ formation. We previously demonstrated that *Wnt4*^{-/-} mouse embryos exhibit NMJ formation defects associated with a decreased number of prepatterned AChR clusters and increased axon outgrowth within the diaphragm (Strochlic et al., 2012). We examined whether *Wnt11*^{-/-} mouse embryos display

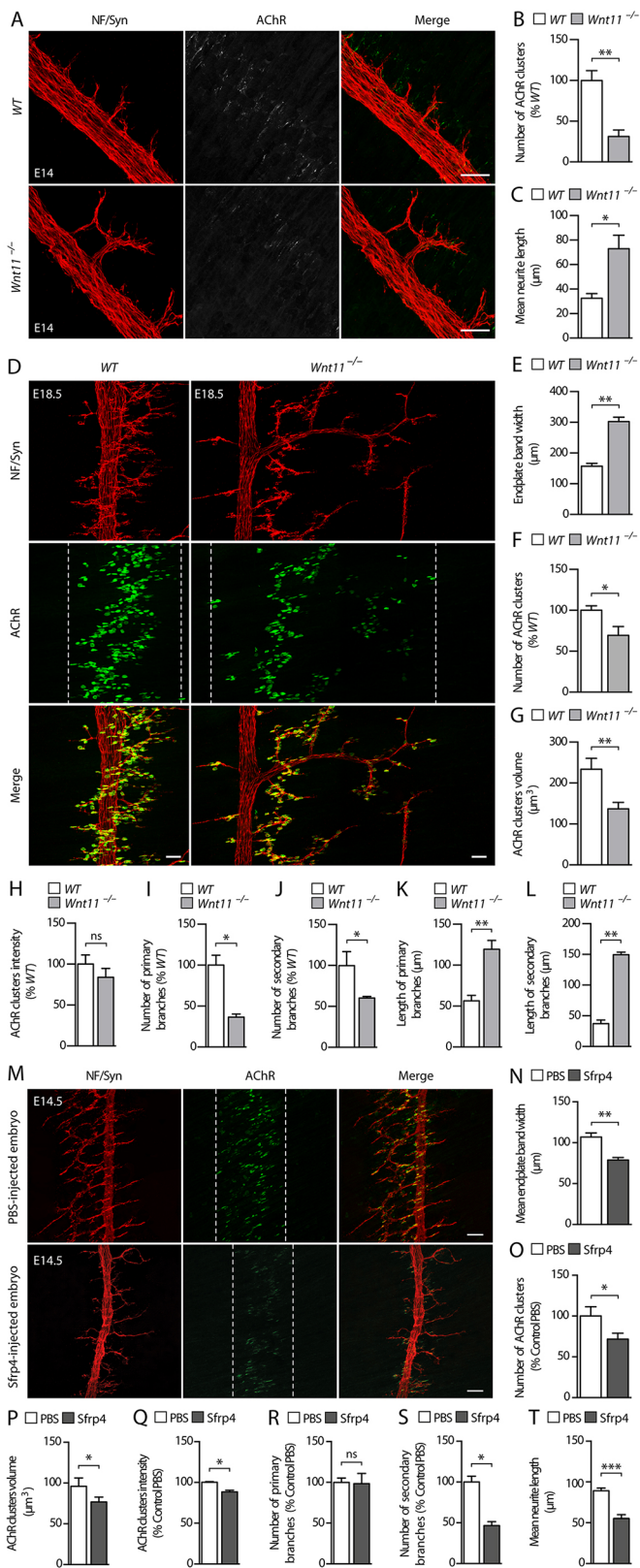


Fig. 3. Loss of Wnt function impairs NMJ formation. (A) Confocal images of whole-mount left hemidiaphragms from E14 WT and *Wnt11*^{-/-} embryos. NF/Syn, red; AChR clusters, green (BTX). (B,C) Quantitative analysis of E14 AChR cluster number (B) and mean axon length (C). (D) Confocal images of whole-mount left hemidiaphragms from E18.5 WT and *Wnt11*^{-/-} embryos stained as in A. White dashed lines delineate the synaptic endplate band. (E-L) Quantification of E18.5 endplate band width (E), AChR cluster number (F), volume (G), fluorescence intensity (H), number of primary (I) and secondary (J) nerve branches, and mean primary (K) and secondary (L) axon length. (M) Confocal images of whole-mount left hemidiaphragms from E14.5 PBS-injected and Sfrp4-injected embryos. NF/Syn, red; AChR clusters, green (BTX). (N-T) Quantification of endplate band width (N), AChR cluster number (O), volume (P), fluorescence intensity (Q), number of primary (R) and secondary (S) nerve branches, and mean axon length (T). ns, non-significant; * $P < 0.05$, ** $P < 0.001$, *** $P < 0.001$. $n = 5$ embryos per condition. Mann-Whitney U -test. Scale bars: 40 μm in A,D,M.

and branches of the phrenic nerve were localized normally in the central region of the muscle as in E14 WT embryos (Fig. 3A), indicating that phrenic axons were able to reach the central and prospective synaptic region of the diaphragm in the absence of Wnt11. However, the number of AChR clusters was reduced by 69% compared with WT (Fig. 3B). In addition, axons were increased in length by 124% in *Wnt11*^{-/-} compared with WT (Fig. 3C). In E18.5 WT embryos, synapses were concentrated in a narrow band and AChR clusters appeared as a thin line in the middle of each hemidiaphragm (Fig. 3D), whereas in *Wnt11*^{-/-} embryos AChR clusters were distributed in a 1.9-fold wider area (Fig. 3D,E). We observed 30% and 42% decreases in cluster number and volume, respectively, in *Wnt11*^{-/-} compared with WT (Fig. 3F-H). In addition to these postsynaptic defects, the presynaptic component was disturbed in *Wnt11*^{-/-} embryos (Fig. 3D). We found 63% and 40% decreases in the number of primary and secondary nerve branches, respectively (Fig. 3I,J). Moreover, instead of ending next to the main phrenic nerve trunk, both primary and secondary branches extended further away from the nerve trunk, with an increase in their length of 112% and 302%, respectively (Fig. 3K,L). Despite this phenotype, nerve terminals were consistently apposed to AChR clusters in *Wnt11*^{-/-} embryos, indicating that Wnt11 is not involved in synapse recognition.

To investigate the effect of Wnt signaling during NMJ formation and to avoid potential redundancy between distinct Wnt ligands, we injected E12.5 mouse embryos with 100 $\mu\text{g}/\text{ml}$ secreted frizzled-related protein 4 (Sfrp4), a Wnt antagonist that serves as a soluble decoy Wnt receptor and thus inhibits all Wnt function and signaling (Ehrlund et al., 2013; He et al., 2005; Park et al., 2008; Surendran et al., 2005). Analysis of NMJ phenotype in Sfrp4-injected embryos at E14.5 revealed that AChR clusters were distributed in a very thin line in the middle of each hemidiaphragm, as compared with PBS-injected embryos (Fig. 3M). The endplate band width was reduced by 22% in Sfrp4-injected embryos compared with the control (Fig. 3N). In addition, the number (-36%), volume (-24%) and intensity (-15%) of AChR clusters were significantly reduced in Sfrp4-injected embryos (Fig. 3O-Q). Interestingly, Sfrp4-injected embryos displayed a drastic loss of terminal arborization. Quantitative analysis revealed that the number of secondary branches in close proximity to the nerve trunk was reduced by 52% and the mean axon length was decreased by 36% in Sfrp4-injected embryos (Fig. 3R-T). Collectively, these data indicate that Wnt proteins contribute to AChR clustering, presynaptic branching and axon outgrowth.

similar NMJ formation defects. Whole-mount diaphragms of E14 and E18.5 *Wnt11*^{-/-} embryos and wild-type (WT) littermates were labeled with BTX together with a mixture of anti-Syn and anti-NF antibodies (Fig. 3A,D). In E14 *Wnt11*^{-/-} embryos, the nerve trunk

Wnt4 and Wnt11 signal through the canonical pathway to elicit AChR clustering and NMJ differentiation

Wnt4 and Wnt11 are known to activate both canonical and non-canonical Wnt signaling, depending on the cell and tissue context

(Heinonen et al., 2011; Lyons et al., 2004; Oteiza et al., 2010; Tao et al., 2005; Toyama et al., 2010). In the canonical pathway, Wnt ligands interact with Fzd receptors and Lrp5/6 co-receptors leading to the neosynthesis of dephosphorylated β -catenin or to the stabilization of cytoplasmic β -catenin which is then dephosphorylated and translocated to the nucleus in order to initiate the transcription of Wnt target genes (Clevers and Nusse, 2012). To evaluate the potential role of Wnt4 and/or Wnt11 in canonical signaling activation in muscle cell cultures, we quantified β -catenin translocation to the nucleus, a classical readout of canonical Wnt signaling. Wnt4 and/or Wnt11 treatment (at maximal concentration for 16 h) resulted in increased levels of cytoplasmic β -catenin and a strong increase in the levels of nuclear β -catenin (Fig. 4A,B,D). We also observed a significant decrease in phosphorylated β -catenin protein levels in the cytoplasm when myotubes were treated simultaneously with Wnt4 and Wnt11 (Fig. 4A,C). Therefore, our data suggest that active β -catenin (non-phosphorylated) is stabilized and translocated to the nucleus in response to Wnt treatment. Moreover, both Wnts significantly increased the fluorescence intensity level of nuclear β -catenin (Fig. 4E,F). Taken together, these results demonstrate that, in muscle cells, Wnt4 and Wnt11 signal through the canonical pathway.

We next asked whether canonical signaling induced by Wnt4 or Wnt11 is required for AChR clustering. We used the secreted Wnt antagonist dickkopf 1 (Dkk1), a specific inhibitor of canonical signaling that binds to Lrp co-receptors, including Lrp4, thus competing with Wnt ligands (Choi et al., 2009; Cruciat and Niehrs, 2013; Niehrs, 2006). Dkk1 treatment reduced the number of Wnt4/Wnt11-induced AChR clusters in a dose-dependent manner, with a maximal effect at 20 ng/ml (−26%, −36% and −57% for Wnt4, Wnt11, and Wnt4 plus Wnt11, respectively; Fig. 4G,H). In addition, Dkk1 (20 ng/ml) impaired nuclear accumulation of β -catenin in myotubes treated with Wnt4 and/or Wnt11, confirming the Dkk1 inhibitory effect (Fig. S2).

In the canonical pathway, β -catenin can function as a transcriptional co-activator through its association with TCF/LEF transcription factors to induce target gene transcriptional programs (MacDonald et al., 2009; Nusse, 2012). We reasoned that Wnt4 and Wnt11 could regulate AChR clustering in part through the canonical pathway-dependent transcriptional activation of AChR subunit genes. Consistent with this hypothesis, mRNA levels of most of the AChR subunits (α , β and γ) were increased in myotubes treated with Wnt4 and Wnt11 as compared with control myotubes (Fig. 4I). Moreover, Dkk1 treatment (20 ng/ml) abolished Wnt-induced increases in the levels of these AChR subunit mRNAs (Fig. 4I). Of note, the mRNA level of the ϵ AChR subunit was not affected by Wnt or Dkk1 treatment, suggesting that this subunit is not a Wnt-responsive target gene.

To further assess the role of Wnt canonical signaling in NMJ formation *in vivo*, we injected Dkk1 (100 μ g/ml) into live embryos (Fig. 4J). AChR clusters were spread throughout a wider muscle area (+16%; Fig. 4K) and the number (−29%) and volume (−24%), but not fluorescence intensity, of AChR clusters were significantly reduced in Dkk1-injected embryos compared with E14.5 PBS-injected controls (Fig. 4L–N). Notably, Dkk1 injections led to aberrant extension (+69%) of motor axons beyond AChR clusters (Fig. 4Q), although the number of primary and secondary branches was unaffected (Fig. 4O,P). Collectively, these data indicate that canonical signaling is required downstream of Wnt4 and Wnt11 to regulate AChR clustering and motor axon outgrowth within the diaphragm.

Strikingly, however, the NMJ phenotype induced by Dkk1 injection did not recapitulate Sfrp4 injection-induced NMJ defects, suggesting that another pathway is required in addition to canonical signaling.

The core PCP component Vangl2 accumulates at developing NMJs and interacts with extracellular Wnt4 and Wnt11, and the Vangl2 loop-tail mutation affects NMJ formation

Given the involvement of Wnt11 in the Wnt/PCP pathway (Gao, 2012), we investigated the role of PCP signaling at the NMJ. We focused on vang-like 2 (Vangl2), one of the most upstream of the core PCP components. Vangl2 is expressed in developing motor axons and is essential for axon guidance in the central nervous system (Avilés and Stoeckli, 2016; Ezan and Montcouquiol, 2013; Nagaoka et al., 2014; Shafer et al., 2011; Tissir and Goffinet, 2013). Moreover, Vangl2 was previously shown to be a postsynaptic protein crucial for synaptogenesis in hippocampal cultures (Nagaoka et al., 2014, 2015). First, we analyzed the pattern of *Vangl2* expression during NMJ formation. We found that *Vangl2* mRNA is highly expressed in diaphragm and hindlimb muscles at E14, when NMJs start to form, and decreases as muscle differentiation proceeds (Fig. 5A). In addition, we identified Vangl2 in protein extracts of E18.5 brain, spinal cord, diaphragm, hindlimb and culture of myotubes (Fig. 5B). Moreover, Vangl2 colocalized with both BTX and the SNARE protein SNAP25, a well-known marker of the presynaptic compartment (Söllner et al., 1993; Washbourne et al., 2002) in E18.5 hindlimb sections, suggesting that Vangl2 is accumulated at the embryonic NMJ (Fig. 5C).

We then tested the potential interaction between Vangl2 and Wnt4 or Wnt11 in a co-culture co-immunoprecipitation assay in which the two partners are expressed by different cells, allowing the detection of extracellular interactions (Yamamoto et al., 2008). Immunoprecipitation was performed after 24 h of co-culture between NIH 3T3 fibroblasts transfected with a plasmid encoding GFP-Vangl2 and HEK 293T cells expressing Wnt11-myc or Wnt4-HA (Fig. 5D). We found that extracellular Wnt4 and Wnt11 co-immunoprecipitated with Vangl2, suggesting that these three proteins are part of a common signaling cascade (Fig. 5E).

To assess the structural consequences of Vangl2 deletion on NMJ formation *in vivo*, we examined the NMJ phenotype of mouse embryos bearing the loop-tail mutation (*Vangl2*^{Lp/Lp}; Fig. 6A,D), which is characterized by a point mutation in the *Vangl2* gene (S464N) that renders the protein ineffective and unstable (Wang et al., 2005). Early during NMJ formation, in E14/E14.5 *Vangl2*^{Lp/Lp} embryos, the number of AChR clusters was reduced by 39% compared with WT, indicating that Vangl2 is required for a normal level of AChR clustering at this early stage (Fig. 6B). Moreover, axons were increased in length by 191% in *Vangl2*^{Lp/Lp} embryos (Fig. 6C). At a later developmental stage (E18.5), AChR clusters were distributed over a wider area and the endplate band width was 1.7-fold larger than in WT littermates (Fig. 6D,E). The number (−34%) and volume (−29%), but not the fluorescence intensity, of *Vangl2*^{Lp/Lp} AChR clusters were reduced compared with WT (Fig. 6F–H). All AChR clusters were innervated in *Vangl2*^{Lp/Lp} embryos (Fig. 6D). However, although the number of both primary and secondary axons was unaffected (Fig. 6I,J), *Vangl2*^{Lp/Lp} embryos showed a striking overextension of secondary motor axon branches (+108%), bypassing AChR clusters and growing aberrantly toward the periphery of the muscle (Fig. 6K,L).

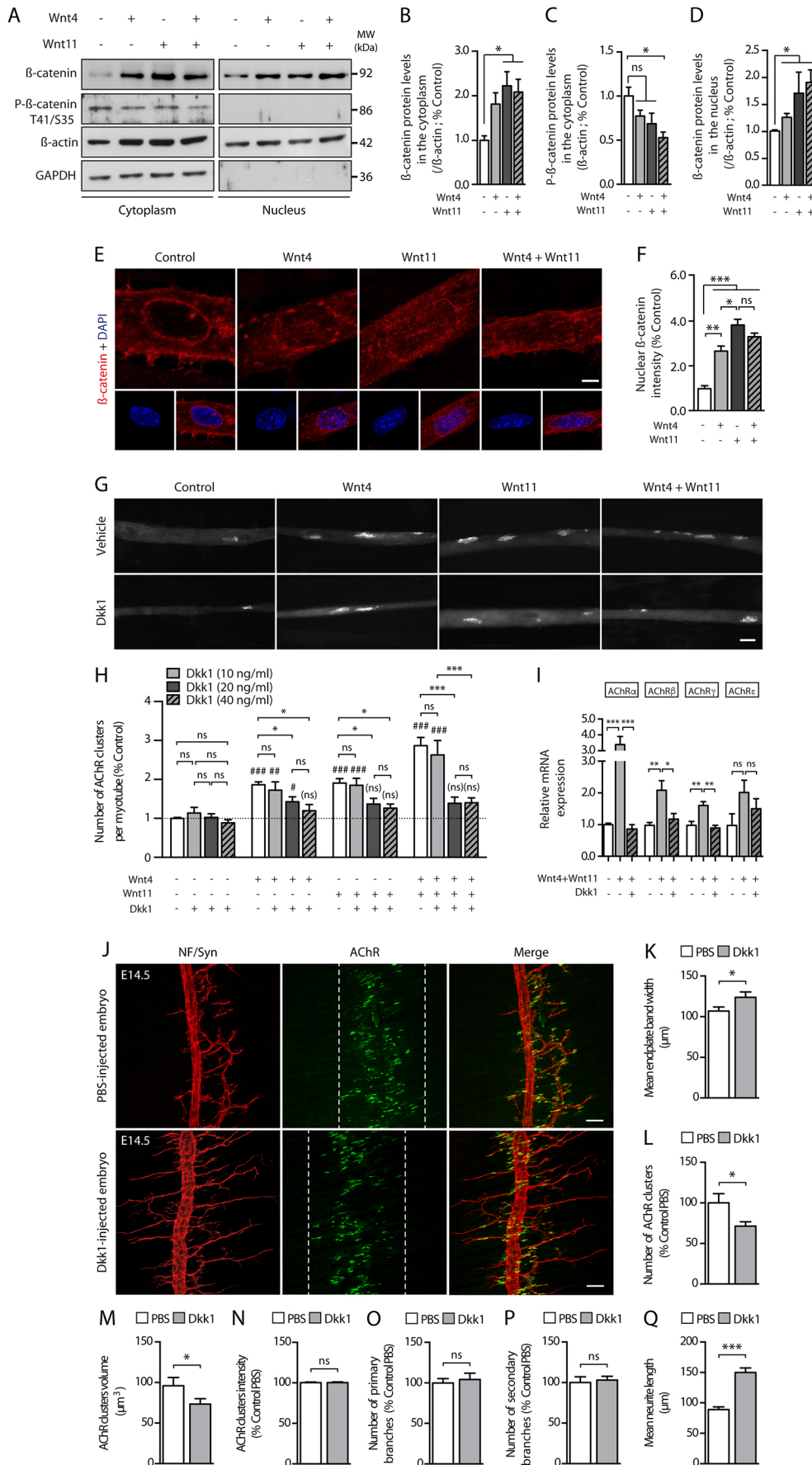


Fig. 4. Wnt4 and Wnt11 signal through the canonical pathway to elicit AChR clustering and NMJ differentiation.

(A) Subcellular protein fractionation of T2 myotubes treated or otherwise with Wnt4 (10 ng/ml) and/or Wnt11 (10 ng/ml). Representative western blot analyses are shown of cytoplasmic and nuclear fractions with phosphorylated (P-β-catenin T41/S35) or total β-catenin antibodies. β-actin was used as a loading control and GAPDH as an indication of cytoplasmic purity. (B,C) Quantification of the total (B) and phosphorylated (C) β-catenin levels normalized to β-actin levels in the cytoplasmic fraction upon control or Wnt treatment. (D) Quantification of total β-catenin levels normalized to β-actin levels in the nuclear fraction upon control or Wnt treatment. (E) Examples of myotubes stained for total β-catenin (red) together with DAPI (blue, nuclei) upon control or Wnt treatment. (F) Quantification of nuclear β-catenin fluorescence intensity upon control or Wnt treatment. (G) Examples of myotubes stained with BTX that were treated with vehicle or Dkk1 (20 ng/ml) in the absence or presence of Wnt4 and/or Wnt11 (10 ng/ml) for 16 h.

(H) Quantification of AChR cluster number in myotubes treated or otherwise with increased concentrations of Dkk1 in the absence or presence of Wnt4 (10 ng/ml) and/or Wnt11 (10 ng/ml). (I) Real-time RT-PCR quantification of relative *AChRα* (*Chra1*), *AChRβ* (*Chrb1*), *AChRγ* (*Chrg*) and *AChRε* (*Chme*) subunit mRNA expression in myotubes treated or otherwise with Wnt4 (10 ng/ml) and/or Wnt11 (10 ng/ml) in the presence or absence of Dkk1 (20 ng/ml).

(J) Confocal images of whole-mount left hemidiaphragms from E14.5 PBS-injected or Dkk1-injected embryos. NF/Syn, red; AChR clusters, green (BTX). White dashed lines delineate the synaptic endplate band. (K-Q) Quantification of endplate band width (K), AChR cluster number (L), volume (M), fluorescence intensity (N), number of primary (O) and secondary (P) nerve branches, and mean axon length (Q). *, #*P*<0.05; **, ###*P*<0.01 and ***, ####*P*<0.001. ns, non-significant. # and (ns): compared with untreated conditions. *n*=6 embryos per condition. Mann-Whitney *U*-test or one-way ANOVA. Scale bars: 10 μm in E; 20 μm in G; 40 μm in J.

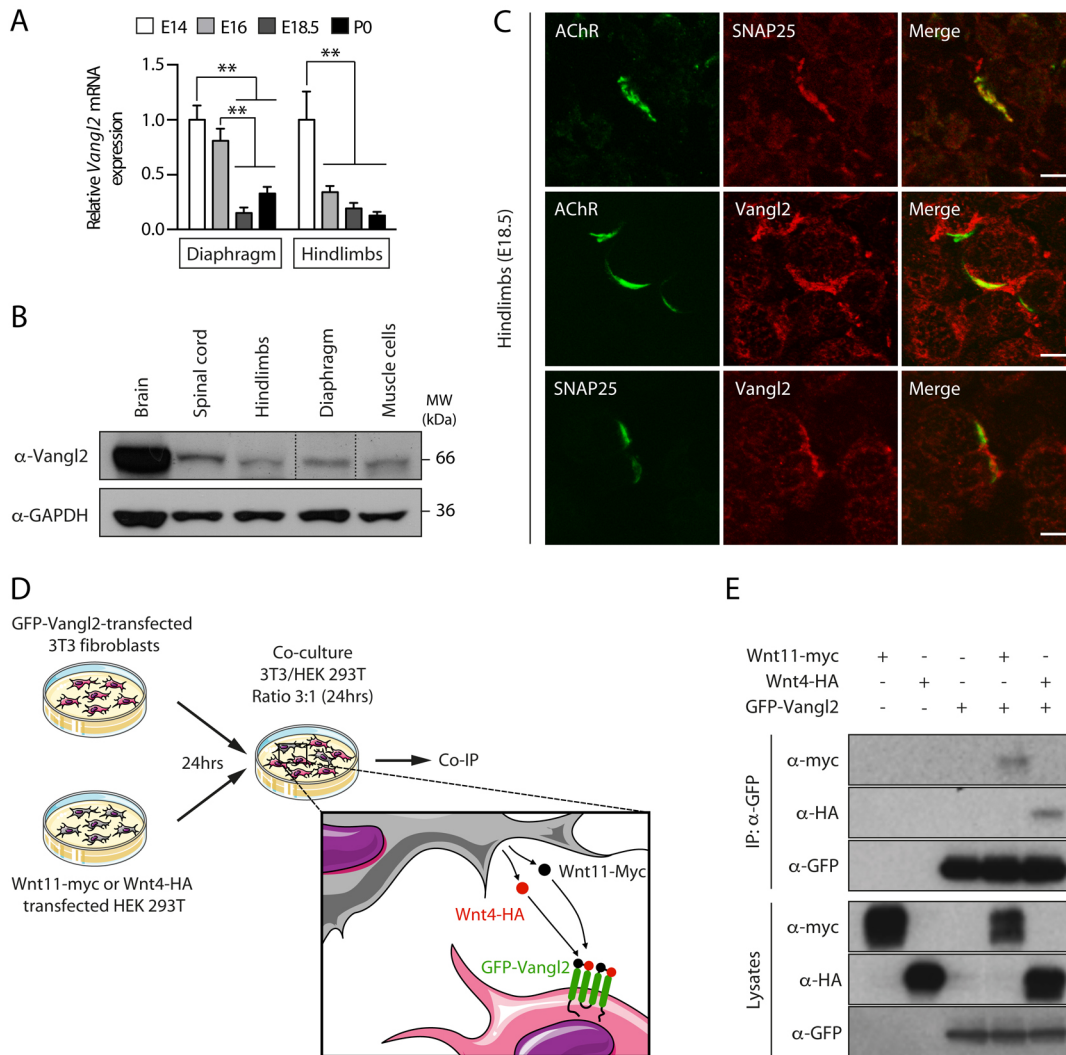


Fig. 5. Vangl2 accumulates at developing NMJs and interacts with extracellular Wnt4 and Wnt11. (A) Real-time RT-PCR quantification of relative *Vangl2* mRNA expression during diaphragm and hindlimb development. (B) Western blot analyses using Vangl2 antibodies of E18.5 brain, spinal cord, diaphragm, hindlimb and muscle cell extracts. GAPDH was used as a loading control. Dotted lines indicate that intervening lanes have been spliced out. (C) E18.5 hindlimb muscle transverse sections stained with SNAP25 (red or green) and/or Vangl2 (red) antibodies with or without BTX (AChR, green). (D) The Wnt4/Wnt11/Vangl2 co-culture co-immunoprecipitation experiment. (E) Co-immunoprecipitation of Wnt11-myc and Wnt4-HA together with GFP-Vangl2 in NIH 3T3/HEK 293T co-culture. Western blots using GFP, HA and myc antibodies were performed on cell lysates to assess the expression of GFP-Vangl2, Wnt4-HA and Wnt11-myc. ** $P < 0.01$; one-way ANOVA. Scale bars: 20 μm .

Since the atypical seven-pass cadherin *Celsr3*, another core component of the PCP signaling pathway, has recently been shown to be involved in limb motor axon guidance (Chai et al., 2014, 2015), we examined whether it could also play a role in NMJ formation. E18.5 *Celsr3*^{-/-} mouse embryos exhibited an NMJ phenotype similar to that of WT littermates, with no pre- or postsynaptic defects (Fig. S3), suggesting that *Celsr3* is dispensable for NMJ formation in the diaphragm muscle. As *Celsr3* mutant mice show a hindlimb phenotype reminiscent of congenital talipes equinovarus (Chai et al., 2015), a possible explanation is that *Celsr3* could function in a subset of motoneurons innervating the hindlimb but not the diaphragm. Alternatively, since three *Celsr* genes/paralogs exist in mammals, the loss of *Celsr3* expression might not be sufficient to alter diaphragm NMJ formation owing to redundancy in *Celsr* function (Tissir and Goffinet, 2013).

In summary, our data demonstrate that Wnt ligands, including Wnt4 and Wnt11, contribute to the process of NMJ formation via

the downstream activation of two pathways – the canonical and a Vangl2-dependent core PCP signaling pathway – to regulate AChR clustering and key aspects of presynaptic differentiation, such as axon branching and outgrowth (Table 1).

DISCUSSION

In this study, we provide evidence that pre- and postsynaptic NMJ differentiation requires a balance of distinct Wnt signaling activities mediated in part by Wnt4 and Wnt11. Based on our findings, we propose that the coordinated action of Wnt4 and Wnt11 activates two downstream signaling pathways, namely the β -catenin-dependent and the Vangl2-dependent PCP pathways, to stimulate AChR cluster formation in the postsynaptic muscle membrane and to regulate presynaptic motor axon outgrowth (Table 1). In addition, our data show that Wnt11 plays a role in presynaptic branching. Our results further highlight the emerging role of Wnt signaling in mammalian NMJ formation and point to distinct roles of Wnt

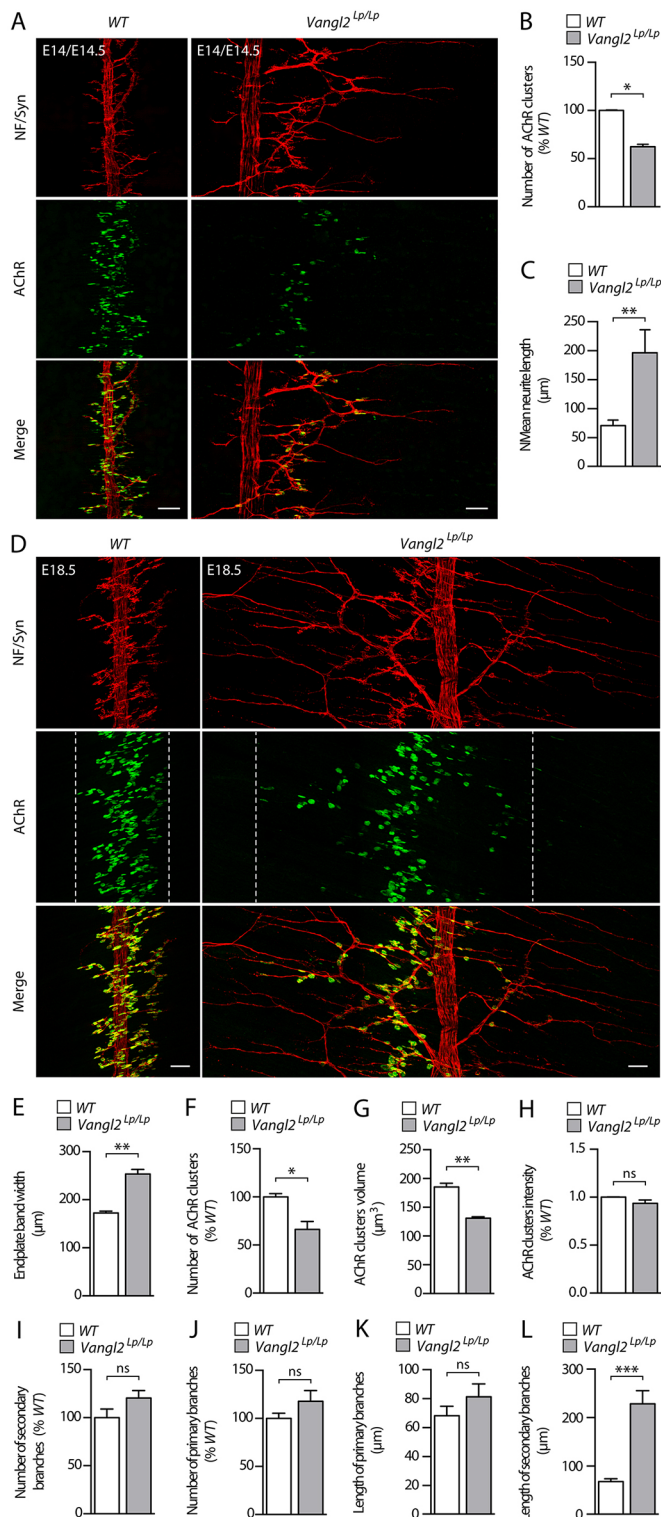


Fig. 6. *Vangl2^{Lp/Lp}* mouse embryos display NMJ formation defects.

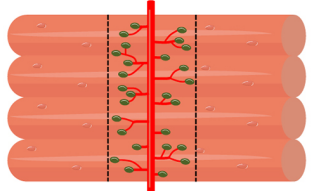
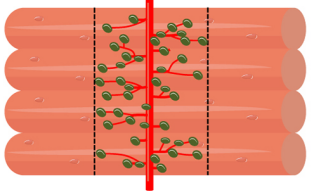
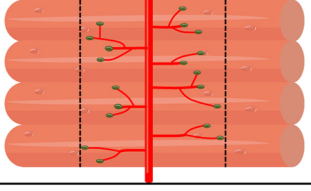
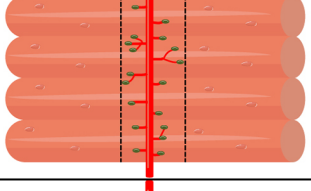
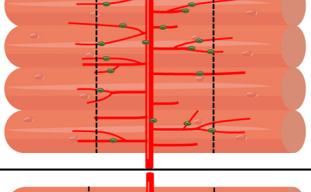
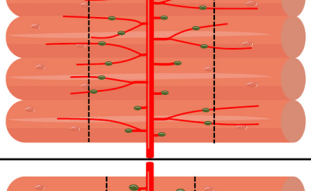
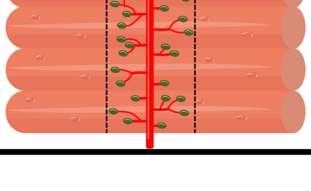
(A) Confocal images of whole-mount left hemidiaphragms from E14/E14.5 WT and *Vangl2^{Lp/Lp}* embryos. NF/Syn, red; AChR clusters, green (BTX). (B,C) Quantification of E14/E14.5 AChR cluster number (B) and mean axon length (C). (D) Confocal images of whole-mount left hemidiaphragms from E18.5 WT and *Vangl2^{Lp/Lp}* embryos stained as in A. White dashed lines delineate the synaptic endplate band. (E–L) Quantification of E18.5 endplate band width (E), AChR cluster number (F), volume (G), fluorescence intensity (H), number of primary (I) and secondary (J) nerve branches, and mean primary (K) and secondary (L) axon length. * $P < 0.05$, ** $P < 0.01$, *** $P < 0.001$; ns, non-significant. $n = 6$ embryos per genotype, Mann–Whitney U -test. Scale bars: 40 μm.

ligands and associated downstream signaling in regulating various aspects of presynaptic differentiation. This is in line with recent advances in Wnt signaling research indicating that the same Wnt can activate different pathways and that several Wnts can mediate one signaling pathway depending on the cell context (Anastas and Moon, 2013).

Coordinated roles of Wnt4 and Wnt11 in AChR clustering

Here, we demonstrate that Wnt4 and Wnt11 cooperate to potentiate their individual postsynaptic activity in muscle cells *in vitro* and in E14.5 injected diaphragm *in vivo*. By contrast, loss of Wnt11 or Wnt-induced signaling in mice severely impairs the early phase of AChR clustering, with a drastic reduction of AChR clusters. *Wnt11* mutant mice were first analyzed at E14 and injected embryos were observed at E14.5, 2 days after injection at E12.5, to visualize the full impact of the injected molecule on the early steps of NMJ formation. E14/E14.5 correspond to the end of the prepatting step, when nerve terminals have reached their muscle target and have started to branch (Tintignac et al., 2015). During this step, early nerve-induced signaling is occurring, many AChR clusters are not yet innervated and both aneural and neural AChR clusters can be visualized and quantified, and thus the AChR defects observed are likely to result from initial nerve-independent postsynaptic differentiation. In line with this, Granato and colleagues showed that both Wnt11r and Wnt4a are required for AChR prepatting in zebrafish and we previously reported that Wnt4 participates in aneural AChR clustering in mice (Gordon et al., 2012; Strohlic et al., 2012). However, only the combined inactivation of *wnt11r* and *wnt4a* in zebrafish led to a complete loss of aneural AChR clusters, and loss of Wnt4 function in mice did not fully abolish muscle prepatting. As in zebrafish, the lack of Wnt11 triggers a more pronounced prepatting defect than Wnt4 deficit. However, the role of Wnt4 and Wnt11 during NMJ formation has been recently challenged by the Burden group, who reported that loss of Wnt11 and/or Wnt4 in mouse embryos did not induce postsynaptic differentiation defects (Remédios et al., 2016). Although, similarly to Remédios et al., our data suggest that neuromuscular synapses are able to form in the absence of Wnt4 and/or Wnt11, strong postsynaptic differentiation defects were quantified revealing that Wnt4 and Wnt11 are key regulators of NMJ formation. In addition, we did not observe the formation of ectopic muscle islands within the central tendon of the diaphragm in *Wnt11* mutant mice. Since distinct genetic backgrounds have been used to breed the *Wnt4* (129Sv/CBA/C57BL/6; Jeays-Ward et al., 2004) and *Wnt11* (C57BL/6/CD1; Cohen et al., 2012) mutant strains, this might explain the discrepancy observed. Indeed, a recent systematic analysis of the phenotype-genotype relationship shows that very different phenotypes can be observed depending on the genetic background for the same null allele (Sittig et al., 2016). In addition, the role of Wnts was investigated using a muscle conditional mutant of *wntless* (*Wls*) in which the secretion of Wnts from muscle is blocked. However, this does not preclude the compensatory secretion of Wnts by other cells. Moreover, several groups have shown that, in addition to Wnt4 and Wnt11, other Wnt proteins are able to stimulate AChR clustering in the absence (Wnt9a, 9b, 10b and 16) or presence (Wnt3) of exogenous neuronal agrin *in vitro* (Barik et al., 2014; Henriquez et al., 2008), suggesting that NMJ formation is likely to require the coordinated function of multiple pro-synaptogenic Wnts and that Wnt functional redundancy and/or compensatory mechanisms that are dependent on the genetic background might also in part explain why single or double Wnt deletion in mice can induce distinct NMJ phenotypes.

Table 1. Summary of NMJ morphological phenotypes in mouse embryos

	AChR clusters		Motor axons			Synaptic band	
	Number	Volume	Number of primary branches	Number of secondary branches	Mean neurite length	Endplate band width	
<i>WT</i>							
<i>Wnt4/Wnt11 GOF</i>	↑	↑	-	-	↑	↑	
<i>Wnt11^{-/-}</i>	↓	↓	↓	↓	I: ↑ II: ↑	↑	
<i>Sfrp4</i>	↓	↓	-	↓	↓	↓	
<i>Dkk1</i>	↓	↓	-	-	↑	↑	
<i>Vangl2^{Lp/Lp}</i>	↓	↓	-	-	I: - II: ↑	↑↑	
<i>Celsr3^{-/-}</i>	-	-	-	-	-	-	

GOF, gain of function; Sfrp4 and Dkk1 refer to direct injections of protein. Arrows indicate increases or decreases relative to wild type (WT), with unchanged indicated by -. I and II refer to primary and secondary nerve branches, respectively. In the diagrams to the right, AChR clusters are in green, the phrenic nerve in red, and black dashed lines delimit the synaptic endplate band width, which includes most AChR clusters.

Our results further indicate that Wnt4/Wnt11-induced AChR clustering in part requires increased levels of AChR subunit gene expression in a β -catenin-dependent manner in muscle cells and that specific inhibition of the canonical pathway *in vivo*, before NMJs start to form, leads to an increased AChR endplate band and to a decrease in the number and volume of AChR clusters. These data demonstrate that Wnt canonical pathway-dependent synaptic gene transcriptional activation is involved in postsynaptic differentiation. Interestingly, mice depleted of β -catenin in muscles displayed similar endplate band width enlargement but divergent AChR cluster size, and no defect in postsynaptic differentiation was detected in muscle β -catenin gain of function (Li et al., 2008; Wu et al., 2012a). Altogether, these data highlight the crucial role of Wnt-elicited canonical signaling in patterning the prospective synaptic endplate band and suggest that a critical level of β -catenin signaling activity is required to regulate AChR cluster formation. In zebrafish, Wnt canonical signaling is not required for AChR clustering and axon guidance (Gordon et al., 2012). This could be related to evolutionary divergence in the role of Wnt signaling between zebrafish and mice.

Both Wnt4 and Wnt11 interact with the MuSK receptor via its Frizzled-like domain (Jing et al., 2009; Strochlic et al., 2012; Zhang et al., 2012). We previously demonstrated that deletion of the MuSK cysteine-rich domain (*MuSKACRD*) in mice altered Wnt11-mediated AChR clustering (Messéant et al., 2015). Moreover, *MuSKACRD* embryos, similarly to Dkk1-injected embryos, exhibited strong defects in postsynaptic differentiation associated with a decrease in AChR cluster numbers, a phenotype that was rescued by forced activation of canonical signaling using lithium chloride (Messéant et al., 2015). Strikingly, no NMJ formation or function defects were found in another mouse line deleted of the MuSK CRD generated by the Burden group (Remédio et al., 2016). Our mice overexpress the mutated MuSK, which could in part explain the difference in the NMJ phenotype observed (Messéant et al., 2015). However, although we do not know what accounts for the difference between the two mouse lines, *MuSKACRD* heterozygous embryos and adults do not display any NMJ phenotype (except a slight increase in axonal length in E14.5 embryos, which is not observed at E18.5), indicating that overexpression of the mutated MuSK is not responsible for the NMJ defects observed (Fig. S4). In addition it is likely that, in contrast to our finding, *MuSKACRD* overexpression would lead to increased AChR clustering and synapse formation, similar to previous results obtained by the Burden group (Kim and Burden, 2008).

Interestingly, our results demonstrate that Wnt4 and Wnt11 also interact with the core PCP protein Vangl2 *in vitro* and that, like *MuSKACRD*, *Vangl2^{Lp/Lp}* embryos display AChR clustering defects suggesting that these four proteins are part of a PCP signaling complex required for AChR accumulation in the postsynaptic membrane. In line with this, Wnt initiation of muscle prepatterning in zebrafish requires MuSK endocytosis and components of the PCP pathway (Gordon et al., 2012; Lacazette et al., 2003). Alternatively, since expression of the Wnt receptor Fzd is largely within the developing diaphragm (Avilés et al., 2014), Vangl2 might signal via an as yet unidentified Fzd receptor to regulate AChR clustering.

Wnt signaling in presynaptic branching and motor axon growth

Our results obtained *in vivo* using specific inhibitors of Wnt signaling suggest that Wnt ligands activate both canonical and

non-canonical pathways that are differentially involved in motor axon outgrowth and nerve branching/arborization. Our data showed that Dkk1-injected embryos and mice bearing the *Vangl2* loop-tail mutation exhibit similar phenotypes, with excessive motor axon growth bypassing AChR clusters, suggesting that both canonical and Vangl2-dependent signaling affect axon outgrowth. Interestingly, a similar phenotype was observed in *MuSKACRD* (Messéant et al., 2015) as well as in Wnt4-deficient (Strochlic et al., 2012) and Wnt11-deficient embryos, although to a lesser extent (no bypassing of AChR clusters in *Wnt11^{-/-}* embryos), suggesting that both Wnts mediate canonical and Vangl2-dependent signaling to regulate this presynaptic phenotype.

It has been shown that muscle-specific but not motoneuronal silencing of β -catenin or Lrp4 expression in mice alters presynaptic differentiation and that muscle β -catenin transcriptional activity is required for presynaptic differentiation, indicating that the presynaptic defects observed in Dkk1-injected mouse embryos are likely to result from inhibition of a muscle canonical retrograde signaling pathway (Li et al., 2008; Liu et al., 2012; Wu et al., 2012b). Since our data show that Vangl2 accumulates at developing NMJs and is likely to be expressed in both presynaptic nerve terminals and postsynaptic muscle domains, it is possible that a Vangl2-dependent signaling is activated in motor axons to regulate and stop the growth of axons once they have reached their target. The role of the PCP pathway in Wnt-induced growth of axons has been well documented (Onishi et al., 2014). However, the similarity between Dkk1- and Vangl2-induced phenotypes raises the interesting hypothesis that both Vangl2 and β -catenin signal in the same pathway. Indeed, endocytosis regulates receptor tyrosine kinase signaling (Goh and Sorkin, 2013) and it has been shown that some of the core PCP proteins are involved in Wnt-induced MuSK internalization and signaling in zebrafish (Gordon et al., 2012). Thus, in this hypothesis, the PCP pathway would act upstream of β -catenin, allowing MuSK endocytosis to trigger activation of Wnt canonical signaling. Alternatively, we cannot exclude the possibility that Vangl2 signals in the Schwann cell to regulate NMJ formation.

In contrast to Dkk1-injected embryos and *Vangl2* mutant phenotypes, and similar to Wnt11 loss of function, transient inhibition of Wnt signaling pathways by Sfrp4 drastically decreases nerve terminal arborization. This suggests that Wnt11 regulates motor axon arborization via an as yet unknown Vangl2-independent and non-canonical Wnt pathway. Whether *Wnt11^{-/-}* AChR clustering defects induce an abnormal presynaptic phenotype or the reverse requires clarification *in vivo*, but it remains clear that Wnt11 directly controls the number of AChR clusters in muscle cells. Whereas *Vangl2* mutant, *Wnt11*-deficient, Dkk1-injected or Sfrp4-injected mouse embryos exhibit the same postsynaptic defects, complex effects specifically affecting arborization or axon outgrowth are observed among the presynaptic phenotypes. Deciphering the presynaptic Wnt-induced mechanisms will require identification of the Wnt receptors and the cell-specific signaling cascades.

MATERIALS AND METHODS

Reagents and mice

The use of animals was in compliance with European Community guidelines (N°A-75-1970). *Wnt11^{-/-}*, *Vangl2^{Lp/Lp}* and *Celsr3^{-/-}* mice were described previously (Majumdar et al., 2003; Montcouquiol et al., 2003; Tissir et al., 2005; Wang et al., 2002). The *Wnt11^{-/-}* strain background is a mixture of C57BL/6 and CD1 (Cohen et al., 2012). Experimental procedures were performed on mutant males and WT

littermates. Information on the reagents and antibodies used is provided in the supplementary Materials and Methods.

RT-PCR

Total RNA from cultured muscle cells, diaphragm or hindlimb muscles free of bones and skin was extracted and RT-PCR analyses using SYBR Green and *Wnt11*, *Vangl2*, *AChRα* (*Chrna1*), *β* (*Chrn1*), *γ* (*Chrn2*) and *ε* (*Chrne*) subunit primers (Qiagen) were performed as described previously (Strochlic et al., 2012). At least three experiments were performed for each muscle cell stage and six embryos were tested for each stage.

Immunoprecipitation and western blot

Subcellular protein fractionation was performed using the Subcellular Fractionation Kit (Thermo Scientific) following the manufacturer's instructions. Transfection (4 μg each plasmid), co-culture co-immunoprecipitation assay and western blot analyses were performed as described previously using the antibodies indicated (Giese et al., 2012; Strochlic et al., 2012; Yamamoto et al., 2008). The co-culture co-immunoprecipitation assay involves the transfection of two potential interactors in two different cell types, followed by co-culture and the immunoprecipitation assay, and provides a simple and reliable method to detect specific protein-protein interactions that occur only in the extracellular space.

Relative signal intensity of total and phosphorylated β-catenin normalized to β-actin was measured using ImageJ software (NIH).

HEK 293T, NIH 3T3 and muscle cell culture

HEK 293T and NIH 3T3 cells (ATCC) were cultured in DMEM (Thermo Scientific) supplemented with 10% fetal bovine serum, 2 mM glutamine and 2% penicillin/streptomycin (500 U) at 37°C in 5% CO₂. The MLCL polyclonal muscle cell line was generated in our laboratory from H-2Kb-tsA58 newborn mouse muscle and was cultured as described previously (Cartaud et al., 2004; Sigoiillot et al., 2010, 2016). Three stages of muscle cell differentiation were selected for analysis: T1, when cells are mostly myotubes (day 0); T2 (day 2), when AChR clusters are visualized; and T3 (day 5), when both AChR and AChE clusters are observed (Guerra et al., 2005). When indicated, recombinant Wnt3a, Wnt4 and/or Wnt11 proteins were added to stage T2 myotubes alone or with Dkk1 for 16 h.

Immunohistochemistry

Staining on whole-mount diaphragms, isolated muscle fibers, tissue sections and myotubes was performed as described previously (Messéant et al., 2015; Strochlic et al., 2012).

Image acquisition and processing

Image acquisition and quantitative analysis of NMJs were performed as previously described (Messéant et al., 2015). Details are provided in the supplementary Materials and Methods.

For quantification of AChR clusters in cultured myotubes, a size threshold was applied such that only AChR clusters of at least 5 μm² were quantified. This allows the detection of AChR aggregates and not AChR micro-clusters, in contrast to quantification made in a previous study (Strochlic et al., 2012), and explains the discrepancy between the results.

Ultrasound-guided microinjection of embryos

WT C57BL/6 pregnant mice at E12.5 (Janvier Labs) were anesthetized (3% isoflurane in air and maintained at 1.5%), installed on a heating pad and monitored for respiration frequency, ECG and temperature (Fig. S1A,B). The pregnant mouse was intraperitoneally injected with Metacam (1 mg/kg body weight; Boehringer Ingelheim). A laparotomy was then performed and the uterine horns were gently exteriorized to allow direct visualization of embryos using an ultrasound biomicroscope (VEVO2100, Visualsonics) equipped with a 60 MHz probe (MS-700; Fig. S1C,D). To ensure contact between the ultrasound probe and the embryos injected, a warm sterile gel (Aquasonic) was used. A quartz micropipette for *in vitro* fertilization (MIC-8-0, Origio; outer diameter 8–10 μm; inner diameter 6.2–7.0 μm) was used to directly inject 5 μl into the embryo, targeting the peritoneum. Visual

observation allowed the identification of any bleeding or ineffective delivery of the injected product (Fig. S1E). At least three embryos were injected per uterine horn, selecting those that were in ideal positions to minimize manipulation of the embryos. The maternal abdomen was then closed using surgery staples, and the injected animals were kept isolated in heated cages 24 h after surgery. Additional injection of Metacam was performed 24 h after surgery.

Wnt4, Wnt11, Sfrp4 and Dkk1 were injected into E12.5 live embryos. The injected embryos were sacrificed at E14.5 and NMJ morphological analyses were performed. Considering the relatively short time frame of the injection (2 days), it is unlikely that any defects observed in the diaphragm would arise from systemic effects.

Statistical analysis

All data are expressed as mean±s.e.m. Statistical analyses were performed and graphs prepared with Prism 6.0 (GraphPad) software. Mann–Whitney *U*-test was used to compare data between two groups. Data of multiple groups were analyzed by one-way ANOVA. Differences were considered significant at *P*<0.05. Each experiment was conducted a minimum of three times.

Acknowledgements

We thank C. Medina, E. Delugré, M. Halliez and M. Boex for technical help; S. Carbonetto for proof reading; and M. Kim, E. Cohen, S. Lefebvre and J. P. Borg for the Wnt11-myc plasmid, *Wnt11*^{-/-} mice, SNAP25 and Vangl2 antibodies, respectively. *In vivo* imaging was performed at the Life Imaging Facility of Paris Descartes University (Plateforme Imageries du Vivant – PIV), supported by Région Ile-de-France research program SESAME.

Competing interests

The authors declare no competing or financial interests.

Author contributions

Conceptualization: C.L., L.S.; Methodology: J.M., C.L., L.S.; Validation: J.M., C.L., L.S.; Formal analysis: J.M., J.E., P.D., K.G., C.M., F.L., G.R., L.S.; Investigation: J.M., K.G., L.S.; Resources: J.E., F.T., M.M., N.S., C.L.; Writing – original draft: J.M., J.E., F.T., M.M., N.S., C.L., L.S.; Writing – review and editing: J.M., J.E., F.T., M.M., N.S., C.L., L.S.; Supervision: C.L., L.S.; Funding acquisition: M.M., N.S., C.L., L.S.

Funding

This work was supported by Association Française contre les Myopathies (AFM) grants 18046 (C.L.) and 14960 (L.S.); Fondation pour la Recherche Médicale (FRM) grant DEQ20160334899; the Centre National de la Recherche Scientifique (CNRS); the Institut National de la Santé et de la Recherche Médicale (INSERM); Université de Bordeaux; and Université Paris Descartes.

Supplementary information

Supplementary information available online at <http://dev.biologists.org/lookup/doi/10.1242/dev.146167.supplemental>

References

- Anastas, J. N. and Moon, R. T. (2013). WNT signalling pathways as therapeutic targets in cancer. *Nat. Rev. Cancer* **13**, 11–26.
- Avilés, E. C. and Stoeckli, E. T. (2016). Canonical wnt signaling is required for commissural axon guidance. *Dev. Neurobiol.* **76**, 190–208.
- Avilés, E. C., Pinto, C., Hanna, P., Ojeda, J., Pérez, V., De Ferrari, G. V., Zamorano, P., Albistur, M., Sandoval, D. and Henríquez, J. P. (2014). Frizzled-9 impairs acetylcholine receptor clustering in skeletal muscle cells. *Front. Cell Neurosci.* **8**, 110.
- Barik, A., Zhang, B., Sohal, G. S., Xiong, W.-C. and Mei, L. (2014). Crosstalk between Agrin and Wnt signaling pathways in development of vertebrate neuromuscular junction. *Dev. Neurobiol.* **74**, 828–838.
- Cartaud, A., Strochlic, L., Guerra, M., Blanchard, B., Lambergeon, M., Krejci, E., Cartaud, J. and Legay, C. (2004). MuSK is required for anchoring acetylcholinesterase at the neuromuscular junction. *J. Cell Biol.* **165**, 505–515.
- Chai, G., Zhou, L., Manto, M., Helmbacher, F., Clotman, F., Goffinet, A. M. and Tissir, F. (2014). Celsr3 is required in motor neurons to steer their axons in the hindlimb. *Nat. Neurosci.* **17**, 1171–1179.
- Chai, G., Goffinet, A. M. and Tissir, F. (2015). Celsr3 and Fzd3 in axon guidance. *Int. J. Biochem. Cell Biol.* **64**, 11–14.
- Choi, H. Y., Dieckmann, M., Herz, J. and Niemeier, A. (2009). Lrp4, a novel receptor for Dickkopf 1 and sclerostin, is expressed by osteoblasts and regulates bone growth and turnover in vivo. *PLoS ONE* **4**, e7930.

- Clevers, H. and Nusse, R. (2012). Wnt/ β -catenin signaling and disease. *Cell* **149**, 1192-1205.
- Cohen, E. D., Miller, M. F., Wang, Z., Moon, R. T. and Morrisey, E. E. (2012). Wnt5a and Wnt11 are essential for second heart field progenitor development. *Development* **139**, 1931-1940.
- Cruciat, C.-M. and Niehrs, C. (2013). Secreted and transmembrane wnt inhibitors and activators. *Cold Spring Harb. Perspect. Biol.* **5**, a015081.
- DeChiara, T. M., Bowen, D. C., Valenzuela, D. M., Simmons, M. V., Poueymirou, W. T., Thomas, S., Kinetz, E., Compton, D. L., Rojas, E., Park, J. S. et al. (1996). The receptor tyrosine kinase MuSK is required for neuromuscular junction formation in vivo. *Cell* **85**, 501-512.
- Ehrlund, A., Mejhert, N., Lorente-Cebrián, S., Åström, G., Dahlman, I., Laurencikiene, J. and Rydén, M. (2013). Characterization of the Wnt inhibitors secreted frizzled-related proteins (SFRPs) in human adipose tissue. *J. Clin. Endocrinol. Metab.* **98**, E503-E508.
- Ezan, J. and Montcouquiol, M. (2013). Revisiting planar cell polarity in the inner ear. *Semin. Cell Dev. Biol.* **24**, 499-506.
- Gao, B. (2012). Wnt regulation of planar cell polarity (PCP). *Curr. Top. Dev. Biol.* **101**, 263-295.
- Giese, A. P., Ezan, J., Wang, L., Lasvaux, L., Lembo, F., Mazzocco, C., Richard, E., Reboul, J., Borg, J.-P., Kelley, M. W. et al. (2012). Gipc1 has a dual role in Vangl2 trafficking and hair bundle integrity in the inner ear. *Development* **139**, 3775-3785.
- Goh, L. K. and Sorkin, A. (2013). Endocytosis of receptor tyrosine kinases. *Cold Spring Harb. Perspect. Biol.* **5**, a017459.
- Gordon, L. R., Gribble, K. D., Syrett, C. M. and Granato, M. (2012). Initiation of synapse formation by Wnt-induced MuSK endocytosis. *Development* **139**, 1023-1033.
- Guerra, M., Cartaud, A., Cartaud, J. and Legay, C. (2005). Acetylcholinesterase and molecular interactions at the neuromuscular junction. *Chem. Biol. Interact.* **157-158**, 57-61.
- He, B., Lee, A. Y., Dadfarmay, S., You, L., Xu, Z., Reguart, N., Mazieres, J., Mikami, I., McCormick, F. and Jablons, D. M. (2005). Secreted frizzled-related protein 4 is silenced by hypermethylation and induces apoptosis in beta-catenin-deficient human mesothelioma cells. *Cancer Res.* **65**, 743-748.
- Heinonen, K. M., Vanegas, J. R., Lew, D., Kroski, J. and Perreault, C. (2011). Wnt4 enhances murine hematopoietic progenitor cell expansion through a planar cell polarity-like pathway. *PLoS ONE* **6**, e19279.
- Henriquez, J. P., Webb, A., Bence, M., Bildsoe, H., Soares, M., Hughes, S. M. and Salinas, P. C. (2008). Wnt signaling promotes AChR aggregation at the neuromuscular synapse in collaboration with agrin. *Proc. Natl. Acad. Sci. USA* **105**, 18812-18817.
- Jeays-Ward, K., Dandonneau, M. and Swain, A. (2004). Wnt4 is required for proper male as well as female sexual development. *Dev. Biol.* **276**, 431-440.
- Jing, L., Lefebvre, J. L., Gordon, L. R. and Granato, M. (2009). Wnt signals organize synaptic prepattern and axon guidance through the zebrafish unplugged/MuSK receptor. *Neuron* **61**, 721-733.
- Kim, N. and Burden, S. J. (2008). MuSK controls where motor axons grow and form synapses. *Nat. Neurosci.* **11**, 19-27.
- Kim, N., Stiegler, A. L., Cameron, T. O., Hallock, P. T., Gomez, A. M., Huang, J. H., Hubbard, S. R., Dustin, M. L. and Burden, S. J. (2008). Lrp4 is a receptor for Agrin and forms a complex with MuSK. *Cell* **135**, 334-342.
- Lacazette, E., Le Calvez, S., Gajendran, N. and Brenner, H. R. (2003). A novel pathway for MuSK to induce key genes in neuromuscular synapse formation. *J. Cell Biol.* **161**, 727-736.
- Li, X.-M., Dong, X.-P., Luo, S.-W., Zhang, B., Lee, D.-H., Ting, A. K. L., Neiswender, H., Kim, C.-H., Carpenter-Hyland, E., Gao, T.-M. et al. (2008). Retrograde regulation of motoneuron differentiation by muscle beta-catenin. *Nat. Neurosci.* **11**, 262-268.
- Liu, Y., Sugiura, Y., Wu, F., Mi, W., Taketo, M. M., Cannon, S., Carroll, T. and Lin, W. (2012). β -Catenin stabilization in skeletal muscles, but not in motor neurons, leads to aberrant motor innervation of the muscle during neuromuscular development in mice. *Dev. Biol.* **366**, 255-267.
- Luo, Z. G., Wang, Q., Zhou, J. Z., Wang, J., Luo, Z., Liu, M., He, X., Wynshaw-Boris, A., Xiong, W. C., Lu, B. et al. (2002). Regulation of AChR clustering by Dishevelled interacting with MuSK and PAK1. *Neuron* **35**, 489-505.
- Lyons, J. P., Mueller, U. W., Ji, H., Everett, C., Fang, X., Hsieh, J.-C., Barth, A. I. M. and McCrea, P. D. (2004). Wnt-4 activates the canonical beta-catenin-mediated Wnt pathway and binds Frizzled-6 CRD: functional implications of Wnt/ β -catenin activity in kidney epithelial cells. *Exp. Cell Res.* **298**, 369-387.
- MacDonald, B. T., Tamai, K. and He, X. (2009). Wnt/ β -catenin signaling: components, mechanisms, and diseases. *Dev. Cell* **17**, 9-26.
- Majumdar, A., Vainio, S., Kispert, A., McMahon, J. and McMahon, A. P. (2003). Wnt11 and Ret/Gdnf pathways cooperate in regulating ureteric branching during metanephric kidney development. *Development* **130**, 3175-3185.
- Messiant, J., Dobbertin, A., Girard, E., Delers, P., Manuel, M., Mangione, F., Schmitt, A., Le Denmat, D., Molgó, J., Zytnicki, D. et al. (2015). MuSK frizzled-like domain is critical for mammalian neuromuscular junction formation and maintenance. *J. Neurosci.* **35**, 4926-4941.
- Montcouquiol, M., Rachel, R. A., Lanford, P. J., Copeland, N. G., Jenkins, N. A. and Kelley, M. W. (2003). Identification of Vangl2 and Scrb1 as planar polarity genes in mammals. *Nature* **423**, 173-177.
- Nagaoka, T., Ohashi, R., Inutsuka, A., Sakai, S., Fujisawa, N., Yokoyama, M., Huang, Y. H., Igarashi, M. and Kishi, M. (2014). The Wnt/planar cell polarity pathway component Vangl2 induces synapse formation through direct control of N-cadherin. *Cell Rep.* **6**, 916-927.
- Nagaoka, T., Tabuchi, K. and Kishi, M. (2015). PDZ interaction of Vangl2 links PSD-95 and Prickle2 but plays only a limited role in the synaptic localisation of Vangl2. *Sci. Rep.* **5**, 12916.
- Niehrs, C. (2006). Function and biological roles of the Dickkopf family of Wnt modulators. *Oncogene* **25**, 7469-7481.
- Nieman, B. J. and Turnbull, D. H. (2010). Ultrasound and magnetic resonance microimaging of mouse development. *Methods Enzymol.* **476**, 379-400.
- Nusse, R. (2012). Wnt signaling. *Cold Spring Harb. Perspect. Biol.* **4**, pii: a011163.
- Onishi, K., Hollis, E. and Zou, Y. (2014). Axon guidance and injury-lessons from Wnts and Wnt signaling. *Curr. Opin. Neurobiol.* **27**, 232-240.
- Oteiza, P., Köppen, M., Krieg, M., Pulgar, E., Farias, C., Melo, C., Preibisch, S., Müller, D., Tada, M., Hartel, S. et al. (2010). Planar cell polarity signalling regulates cell adhesion properties in progenitors of the zebrafish laterality organ. *Development* **137**, 3459-3468.
- Packard, M., Koo, E. S., Gorczyca, M., Sharpe, J., Cumberledge, S. and Budnik, V. (2002). The Drosophila Wnt, wingless, provides an essential signal for pre- and postsynaptic differentiation. *Cell* **111**, 319-330.
- Park, J.-R., Jung, J.-W., Lee, Y.-S. and Kang, K.-S. (2008). The roles of Wnt antagonists Dkk1 and sFRP4 during adipogenesis of human adipose tissue-derived mesenchymal stem cells. *Cell Prolif.* **41**, 859-874.
- Remédios, L., Gribble, K. D., Lee, J. K., Kim, N., Hallock, P. T., Delestrée, N., Mentis, G. Z., Froemke, R. C., Granato, M. and Burden, S. J. (2016). Diverging roles for Lrp4 and Wnt signaling in neuromuscular synapse development during evolution. *Genes Dev.* **30**, 1058-1069.
- Shafer, B., Onishi, K., Lo, C., Colakoglu, G. and Zou, Y. (2011). Vangl2 promotes Wnt/planar cell polarity-like signaling by antagonizing Dvl1-mediated feedback inhibition in growth cone guidance. *Dev. Cell* **20**, 177-191.
- Sigoillot, S. M., Bourgeois, F., Lambergeon, M., Strohlic, L. and Legay, C. (2010). ColQ controls postsynaptic differentiation at the neuromuscular junction. *J. Neurosci.* **30**, 13-23.
- Sigoillot, S. M., Bourgeois, F., Karmouch, J., Molgó, J., Dobbertin, A., Chevalier, C., Houlgatte, R., Léger, J. and Legay, C. (2016). Neuromuscular junction immaturity and muscle atrophy are hallmarks of the ColQ-deficient mouse, a model of congenital myasthenic syndrome with acetylcholinesterase deficiency. *FASEB J.* **30**, 2382-2399.
- Sittig, L. J., Carbonetto, P., Engel, K. A., Krauss, K. S., Barrios-Camacho, C. M. and Palmer, A. A. (2016). Genetic background limits generalizability of genotype-phenotype relationships. *Neuron* **91**, 1253-1259.
- Slevin, J. C., Byers, L., Gertsenstein, M., Qu, D., Mu, J., Sunn, N., Kingdom, J. C. P., Rossant, J. and Adamson, S. L. (2006). High resolution ultrasound-guided microinjection for interventional studies of early embryonic and placental development in vivo in mice. *BMC Dev. Biol.* **6**, 10.
- Söllner, T., Whiteheart, S. W., Brunner, M., Erdjument-Bromage, H., Geromanos, S., Tempst, P. and Rothman, J. E. (1993). SNAP receptors implicated in vesicle targeting and fusion. *Nature* **362**, 318-324.
- Strohlic, L., Falk, J., Goillot, E., Sigoillot, S., Bourgeois, F., Delers, P., Rouvière, J., Swain, A., Castellani, V., Schaeffer, L. et al. (2012). Wnt4 participates in the formation of vertebrate neuromuscular junction. *PLoS ONE* **7**, e29976.
- Surendran, K., Schiavi, S. and Hruska, K. A. (2005). Wnt-dependent beta-catenin signaling is activated after unilateral ureteral obstruction, and recombinant secreted frizzled-related protein 4 alters the progression of renal fibrosis. *J. Am. Soc. Nephrol.* **16**, 2373-2384.
- Tao, Q., Yokota, C., Puck, H., Kofron, M., Birsoy, B., Yan, D., Asashima, M., Wylie, C. C., Lin, X. and Heasman, J. (2005). Maternal Wnt11 activates the canonical Wnt signaling pathway required for axis formation in xenopus embryos. *Cell* **120**, 857-871.
- Tintignac, L. A., Brenner, H.-R. and Rüegg, M. A. (2015). Mechanisms regulating neuromuscular junction development and function and causes of muscle wasting. *Physiol. Rev.* **95**, 809-852.
- Tissir, F. and Goffinet, A. M. (2013). Shaping the nervous system: role of the core planar cell polarity genes. *Nat. Rev. Neurosci.* **14**, 525-535.
- Tissir, F., Bar, I., Jossin, Y., De Backer, O. and Goffinet, A. M. (2005). Protocadherin Celsr3 is crucial in axonal tract development. *Nat. Neurosci.* **8**, 451-457.
- Toyama, T., Lee, H. C., Koga, H., Wands, J. R. and Kim, M. (2010). Noncanonical Wnt11 inhibits hepatocellular carcinoma cell proliferation and migration. *Mol. Cancer Res.* **8**, 254-265.
- Wang, J. and Luo, Z.-G. (2008). The role of Wnt/ β -catenin signaling in postsynaptic differentiation. *Commun. Integr. Biol.* **1**, 158-160.
- Wang, Y., Thekdi, N., Smallwood, P. M., Macke, J. P. and Nathans, J. (2002). Frizzled-3 is required for the development of major fiber tracts in the rostral CNS. *J. Neurosci.* **22**, 8563-8573.

- Wang, J., Mark, S., Zhang, X., Qian, D., Yoo, S.-J., Radde-Gallwitz, K., Zhang, Y., Lin, X., Collazo, A., Wynshaw-Boris, A. et al. (2005). Regulation of polarized extension and planar cell polarity in the cochlea by the vertebrate PCP pathway. *Nat. Genet.* **37**, 980-985.
- Wang, J., Ruan, N.-J., Qian, L., Lei, W.-L., Chen, F. and Luo, Z.-G. (2008). Wnt/ beta-catenin signaling suppresses Rapsyn expression and inhibits acetylcholine receptor clustering at the neuromuscular junction. *J. Biol. Chem.* **283**, 21668-21675.
- Wang, J.-Y., Chen, F., Fu, X.-Q., Ding, C.-S., Zhou, L., Zhang, X.-H. and Luo, Z.-G. (2014). Caspase-3 cleavage of dishevelled induces elimination of postsynaptic structures. *Dev. Cell* **28**, 670-684.
- Washbourne, P., Thompson, P. M., Carta, M., Costa, E. T., Mathews, J. R., Lopez-Bendito, G., Molnár, Z., Becher, M. W., Valenzuela, C. F., Partridge, L. D. et al. (2002). Genetic ablation of the t-SNARE SNAP-25 distinguishes mechanisms of neuroexocytosis. *Nat. Neurosci.* **5**, 19-26.
- Weatherbee, S. D., Anderson, K. V. and Niswander, L. A. (2006). LDL-receptor-related protein 4 is crucial for formation of the neuromuscular junction. *Development* **133**, 4993-5000.
- Wu, H., Lu, Y., Barik, A., Joseph, A., Taketo, M. M., Xiong, W.-C. and Mei, L. (2012a). β -Catenin gain of function in muscles impairs neuromuscular junction formation. *Development* **139**, 2392-2404.
- Wu, H., Lu, Y., Shen, C., Patel, N., Gan, L., Xiong, W. C. and Mei, L. (2012b). Distinct roles of muscle and motoneuron LRP4 in neuromuscular junction formation. *Neuron* **75**, 94-107.
- Wu, H., Barik, A., Lu, Y., Shen, C., Bowman, A., Li, L., Sathyamurthy, A., Lin, T. W., Xiong, W.-C. and Mei, L. (2015). Slit2 as a β -catenin/Ctnnb1-dependent retrograde signal for presynaptic differentiation. *eLife* **4**, doi: 10.7554/eLife.07266.
- Yamamoto, S., Nishimura, O., Misaki, K., Nishita, M., Minami, Y., Yonemura, S., Tarui, H. and Sasaki, H. (2008). Cthrc1 selectively activates the planar cell polarity pathway of Wnt signaling by stabilizing the Wnt-receptor complex. *Dev. Cell* **15**, 23-36.
- Zhang, B., Luo, S., Wang, Q., Suzuki, T., Xiong, W. C. and Mei, L. (2008). LRP4 serves as a coreceptor of agrin. *Neuron* **60**, 285-297.
- Zhang, W., Coldefy, A.-S., Hubbard, S. R. and Burden, S. J. (2011). Agrin binds to the N-terminal region of Lrp4 protein and stimulates association between Lrp4 and the first immunoglobulin-like domain in muscle-specific kinase (MuSK). *J. Biol. Chem.* **286**, 40624-40630.
- Zhang, B., Liang, C., Bates, R., Yin, Y., Xiong, W.-C. and Mei, L. (2012). Wnt proteins regulate acetylcholine receptor clustering in muscle cells. *Mol. Brain* **5**, 7.
- Zong, Y., Zhang, B., Gu, S., Lee, K., Zhou, J., Yao, G., Figueiredo, D., Perry, K., Mei, L. and Jin, R. (2012). Structural basis of agrin-LRP4-MuSK signaling. *Genes Dev.* **26**, 247-258.

Supplemental Materials and Methods

Reagents and antibodies

The following antibodies and reagents were used: α -bungarotoxin Alexa Fluor[®] 488 conjugate (B13422, Life Technologies, 1/1000), anti-synaptophysin (08-0130, Invitrogen, 1/5), anti-neurofilament 68 kDa (AB9568, Millipore, 1/750), anti-SNAP25 (HPA001830, Sigma, 1/500), anti-HA (901514, BioLegend, 1/2500), anti- β -catenin (610153, BD Biosciences, 1/1000), anti-phospho β -catenin (phospho T41 + S45) (ab38511, Abcam, 1/500); anti- β -actin (ab8227, Abcam, 1/3000); anti-GAPDH (ab9485, Abcam, 1/5000); anti-GFP (11814460001, Roche, 1/500); anti-Myc (2276S, Ozyme, 1/500). Dkk1, Sfrp4, Wnt3a, Wnt4 and Wnt11 proteins were purchased from R&D Systems. Polyclonal (1/500 for western blot) and monoclonal (1/200 for immunostaining) anti-Vangl2 have been previously described (Montcouquiol et al., 2006; Puvirajesinghe et al., 2016).

Images acquisition and processing.

All images were collected on a microscope (model BX61; Olympus) equipped with a Fast 1394 Digital CCD FireWire camera or on a confocal laser scanning microscope (Zeiss LSM-710). The same laser power and parameter setting were applied to ensure fair comparison between WT and mutant muscles. Confocal images presented are single-projected image derived from overlaying each set of collected Z-stacks. For quantification of the AChR clusters number, volume and intensity, image stacks were quantified using the ImageJ (version 1.46m) plugin “3D object counter” (Bolte and Cordelières, 2006). The threshold intensity was set by visual inspection of AChR clusters, being the same between WT and mutant images. The endplate band width was defined by the distance between the two farthest AChR clusters from the main nerve trunk. Around 100 measurements regularly spaced and covering the entire diaphragm were taken. For presynaptic quantification, the number and length of primary and secondary branches were performed from at least 6 single-projected

images per genotype using ImageJ software. Primary and secondary branches were defined as axons that extended from the main nerve trunk (primary) or from the primary branches (secondary). For analyses of E14/E14.5 injected-embryos, since secondary branches were not fully differentiated, we quantified the mean axon length defined as the total length of the axons that extended from the nerve trunk. At least 4 diaphragms or 50 isolated muscle fibers of each genotype were analyzed and quantified. To evaluate β -catenin translocation to nuclei in myotubes, image stacks corresponding to nuclei were used for quantification using the ImageJ intensity plot profile.

Supplemental references

Bolte, S. and Cordelières, F. P. (2006). A guided tour into subcellular colocalization analysis in light microscopy. *J. Microsc.* **224**, 213–232.

Montcouquiol, M., Sans, N., Huss, D., Kach, J., Dickman, J. D., Forge, A., Rachel, R. A., Copeland, N. G., Jenkins, N. A., Bogani, D., et al. (2006). Asymmetric localization of Vangl2 and Fz3 indicate novel mechanisms for planar cell polarity in mammals. *J. Neurosci. Off. J. Soc. Neurosci.* **26**, 5265–5275.

Puvirajesinghe, T. M., Bertucci, F., Jain, A., Scerbo, P., Belotti, E., Audebert, S., Sebbagh, M., Lopez, M., Brech, A., Finetti, P., et al. (2016). Identification of p62/SQSTM1 as a component of non-canonical Wnt VANGL2-JNK signalling in breast cancer. *Nat. Commun.* **7**, 10318.

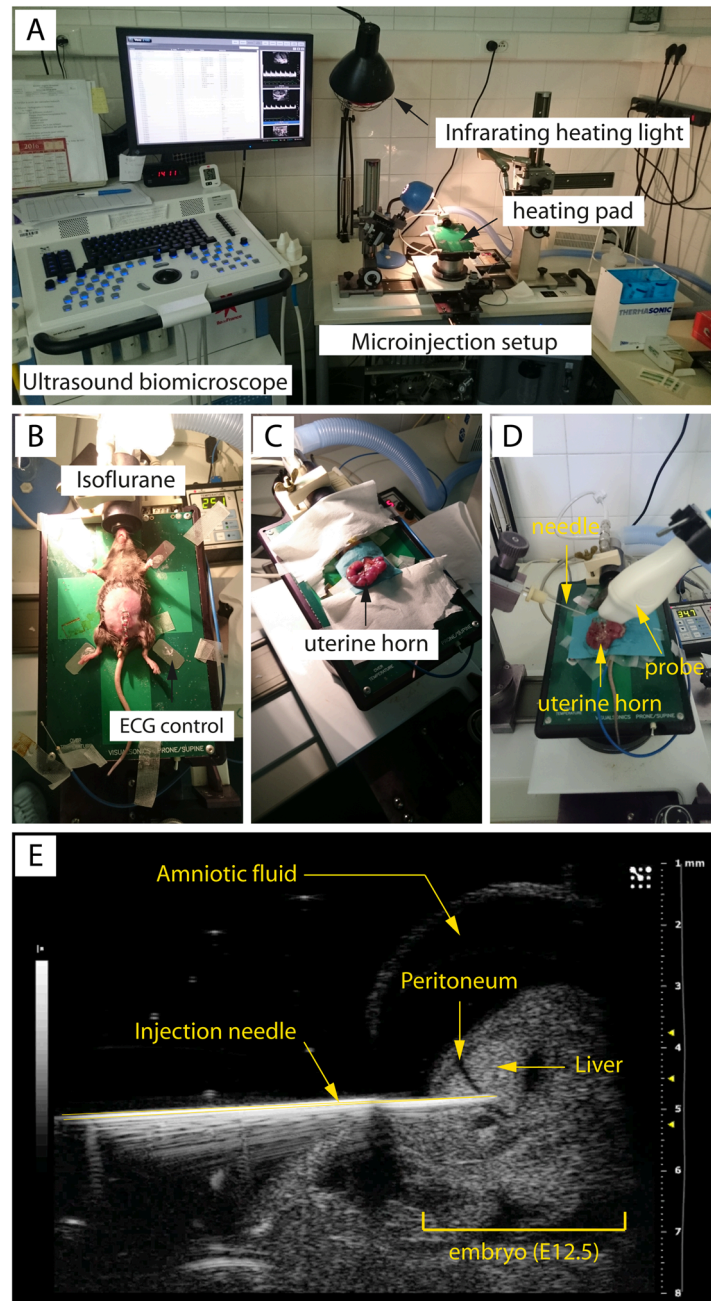


Figure S1.

Figure S1. Setup for ultrasound-guided injections in live mice embryos.

(A) Photography showing the heating pad on which the anesthetized pregnant mouse was installed and the ultrasound biomicroscope. Additional eating of the animal was ensured with an infrared eating light all along the experiment. (B) Monitoring respiration frequency, ECG and temperature of the mouse was performed. (C) A laparotomy was performed and the uterine horns were gently exteriorized. (D) A warm sterile gel was used to ensure contact between the ultrasound probe and the embryos (E12.5). Quartz micropipette for *in vitro*

fertilization was used to inject into the embryo together with the Visualsonics microinjection positioning system. **(E)** Example of an ultrasound image showing a microinjection performed directly in the embryo peritoneum. Note that the peritoneum is identified depending on the location of the liver.

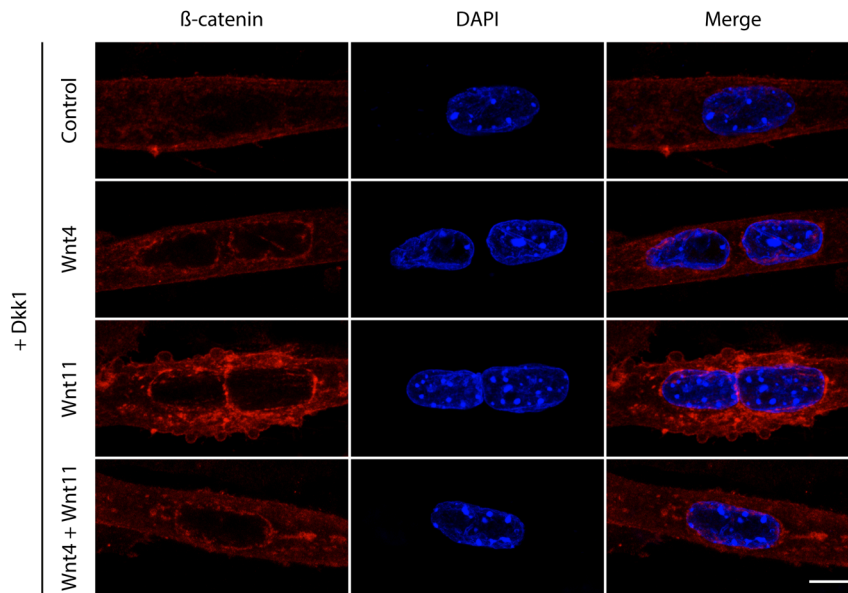


Figure S2.

Figure S2. Dkk1 impairs β -catenin nuclear accumulation in myotubes treated with Wnt4 and/or Wnt11.

Examples of myotubes stained with total β -catenin (red) together with DAPI (blue, nuclei) treated with Dkk1 (20 ng/ml) in the absence or presence of Wnt4 and/or Wnt11 (10 ng/ml). Scale bar in the merged image, 10 μ m.

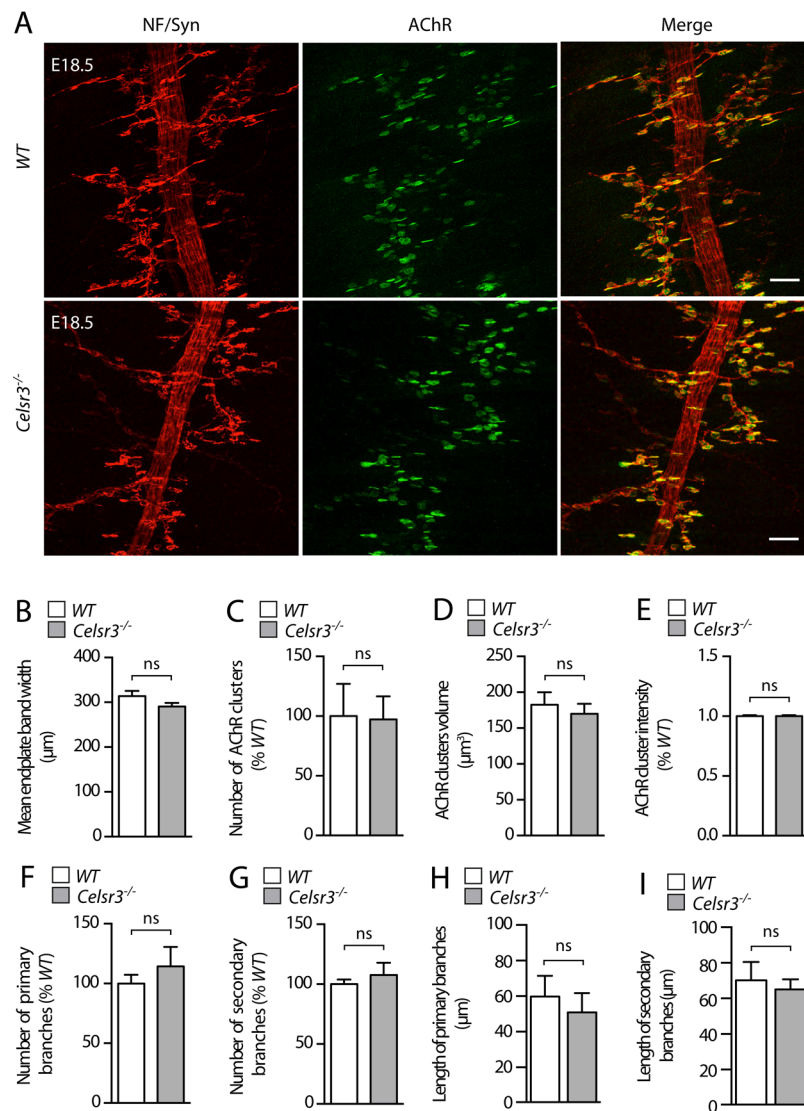


Figure S3.

Figure S3. *Celsr3* is dispensable for NMJ formation in diaphragms.

(A) Confocal images of whole mount left hemidiaphragms from E18.5 *WT* and *Celsr3*^{-/-} embryos stained with neurofilament (NF, red) and synaptophysin (Syn, red) antibodies together with α -BTX (AChRs, green). (B-I) Quantitative analysis of the endplate band width (B), the AChR clusters number (C), volume (D), fluorescence intensity (E), the number of primary (F) and secondary (G) nerve branches and the mean primary (H) and secondary (I) neurite length. Data are shown as mean \pm SEM. ns, non significant. N = 5 embryos per genotype, Mann-Whitney U test. Scale bar in the merged image in A, 50 μ m.

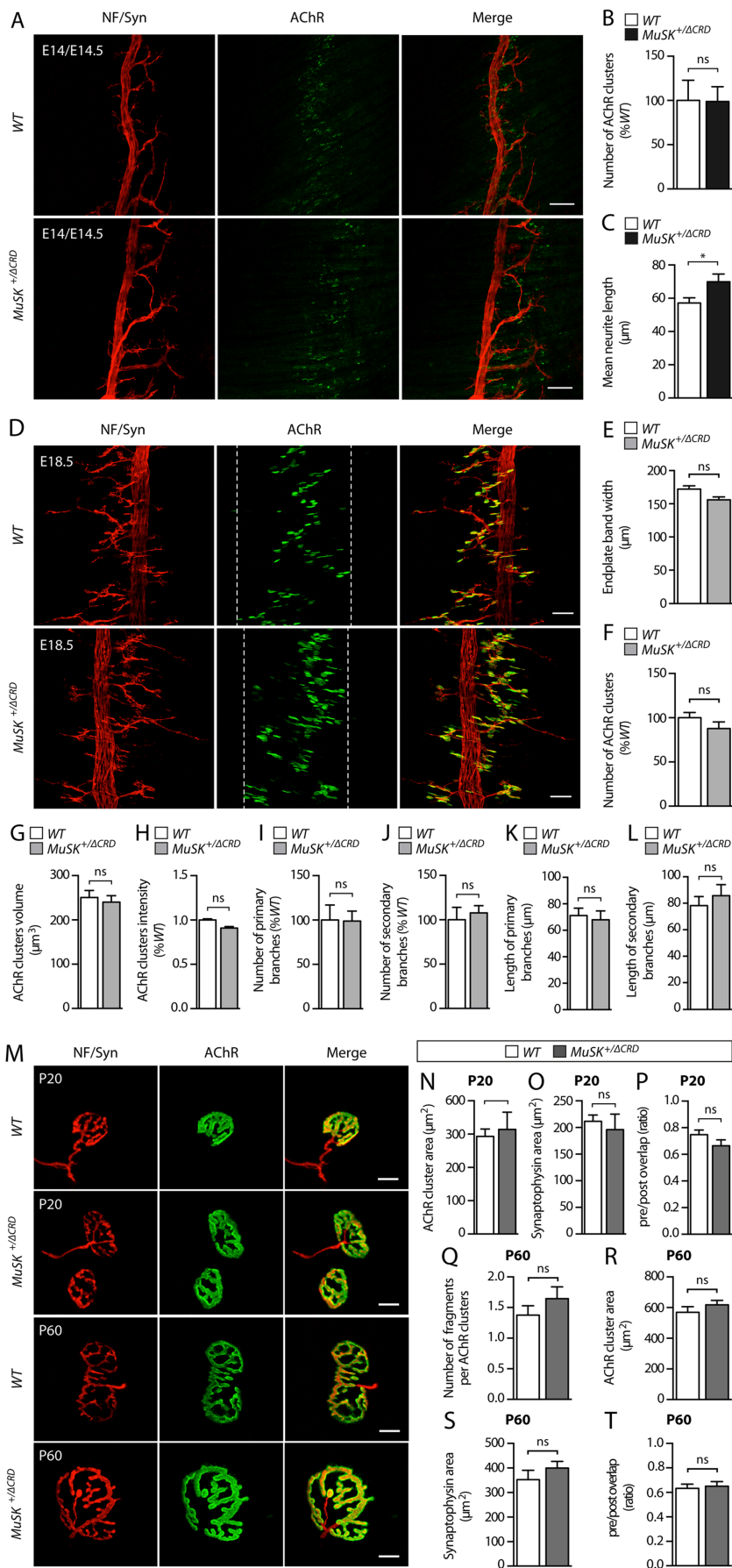


Figure S4.

Figure S4. Identical NMJ phenotypes between *WT* and *MuSK*^{+/ Δ CRD} mice during synapse formation and maturation.

(A) Confocal images of whole mount left hemidiaphragms from E14/E14.5 *WT* and *MuSK*^{+/ Δ CRD} embryos stained with neurofilament (NF, red) and synaptophysin (Syn, red) antibodies together with α -BTX (green). **(B and C)** Quantitative analysis of the E14/E14.5 AChR clusters number (B) and mean neurite length (C). **(D)** Confocal images of whole mount left hemidiaphragms from E18.5 *WT* and *MuSK*^{+/ Δ CRD} embryos stained as in A. White dashed lines delineate the synaptic endplate band. **(E-L)** Quantitative analysis of the E18.5 endplate band width (E), the AChR clusters number (F), volume (G), fluorescence intensity (H), the number of primary (I) and secondary (J) nerve branches and the mean primary (K) and secondary (L) neurite length. **(M)** Confocal images of whole mount isolated muscle fibers from P20 and P60 *WT* and *MuSK*^{+/ Δ CRD} Tibialis Anterior, stained as in A. **(N-P)** Quantitative analysis of the AChR cluster area (N), the Syn area (O), and overlap area of presynaptic and postsynaptic elements (P) in P20 *WT* and *MuSK*^{+/ Δ CRD} mice. **(Q-T)** Quantitative analysis of the number of fragments per AChR cluster (Q), the AChR cluster area (R), the Syn area (S), and the overlap ratio of presynaptic and postsynaptic elements (T) in P60 *WT* and *MuSK*^{+/ Δ CRD} mice. * $p < 0.05$; ns, non significant. Mann-Whitney U test. N=4 embryos or animals per condition. Scale bar in the merged image in A and D, 40 μ m; in M, 10 μ m.